iScience

Article

miR-193b-365 microcluster downstream of *Fezf2* coordinates neuron-subtype identity and dendritic morphology in cortical projection neurons

Graphical abstract

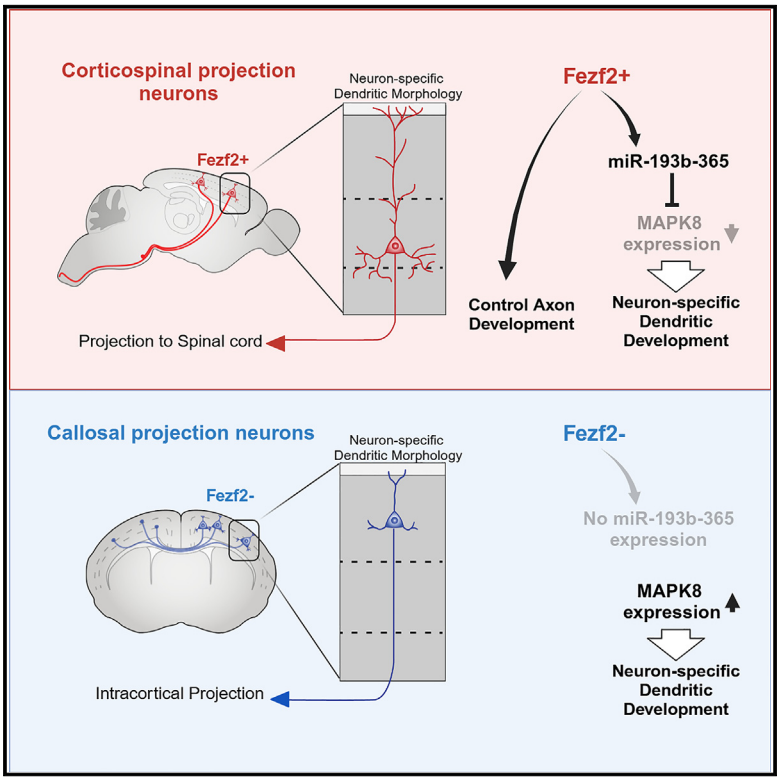

Highlights

- miR-193b∼365 microRNA cluster is enriched in corticospinal neurons
- miR-193b∼365 is regulated by *Fezf2* and repress MAPK8 in corticospinal neuron
- MAPK8 regulation via miR-193b∼365 controls neuron-specific dendritic morphology

Authors

Asha Iyer, Lee O. Vaasjo, Verl B. Siththanandan, ..., Ramesh Nair, Maria J. Galazo, Suzanne Tharin

Correspondence

mgalazo@tulane.edu

In brief

Biological sciences; Epigenetics; Developmental neuroscience

Iyer et al., 2024, iScience *27*, 111500
December 20, 2024 © 2024 The Authors. Published by Elsevier Inc.
https://doi.org/10.1016/j.isci.2024.111500

CellPress

iScience

CellPress
OPEN ACCESS

Article

miR-193b-365 microcluster downstream of *Fezf2* coordinates neuron-subtype identity and dendritic morphology in cortical projection neurons

Asha Iyer,[1,7] Lee O. Vaasjo,[2,7] Verl B. Siththanandan,[1] Rajan K C,[5] Abbigail Thurmon,[5] Mauren Akumuo,[5] Victoria Lu,[1] Chelsea Nnebe,[1,6] Ramesh Nair,[3] Maria J. Galazo,[2,5,8,9,*] and Suzanne Tharin[1,4,6,8]

[1]Department of Neurosurgery, Stanford University, Stanford, CA 94305, USA
[2]Neuroscience program, Tulane Brain Institute, Tulane University, New Orleans, LA 70118 USA
[3]Stanford Center for Genomics and Personalized Medicine, Stanford, CA 94305, USA
[4]Division of Neurosurgery, Palo Alto Veterans Affairs Health Care System, Palo Alto, CA 94304, USA
[5]Department of Cell and Molecular Biology, Tulane University, New Orleans, LA 70118 USA
[6]Neurosciences PhD program, Stanford University, Stanford, CA 94305, USA
[7]These authors contributed equally
[8]Senior author
[9]Lead contact
*Correspondence: mgalazo@tulane.edu
https://doi.org/10.1016/j.isci.2024.111500

SUMMARY

Different neuron types develop characteristic axonal and dendritic arborizations that determine their inputs, outputs, and functions. Expression of fate-determinant transcription factors is essential for specification of their distinct identities. However, the mechanisms downstream of fate-determinant factors coordinating different aspects of neuron identity are not understood. Specifically, how distinct projection neurons develop appropriate dendritic arbors that determine their inputs is unknown. Here, we investigate this question in corticospinal and callosal projection neurons. We identified a mechanism linking the corticospinal/corticofugal identity gene *Fezf2* with the regulation of dendritic development. We show that miR-193b∼365 microRNA cluster is regulated by *Fezf2* and enriched in corticospinal neurons. miR-193b∼365 represses mitogen-activated protein kinase 8 (MAPK8) to regulate corticospinal dendritic development. miR-193b∼365 overexpression in callosal neurons abnormally reduces MAPK8 signal and dendritic complexity. Our findings show that regulation of MAPK8 via miR-193b∼365 cluster regulates dendritic development, providing a mechanism that coordinates projection neuron identity, specified by *Fezf2*, and neuron-specific dendritic morphology.

INTRODUCTION

The six-layered mammalian neocortex is generated in an inside-out fashion, with the earlier-born corticofugal projection neurons populating the deep cortical layers, and the later-born corticocortical projection neurons populating the superficial layers.[1] Each of these broad classes of projection neurons has distinct characteristics, including gene expression, axonal projections, dendritic morphology, and electrophysiological properties that collectively define their identity and function.[2,3] Substantial progress has been made in understanding the genetic programs regulating identity specification of these broad classes of cortical projection neurons.[2,4,5] Key transcription factors controlling identity acquisition in these subtypes of projection neurons have been revealed.[2–4,6,7] However, the logic governing the coordinated gene regulation downstream of these transcription factors to control and execute the distinct characteristics that define an individual neuronal subtype is still unknown. For example, how molecules controlling the characteristic axon projection pattern and the dendritic field of each projection neuron subtype are coordinated is still unknown. This coordination is critical to establish the distinct inputs, outputs, and therefore the distinct functions of each neuron subtype.

Corticospinal projection neurons and interhemispheric callosal projection neurons are among the best-characterized neuron subtypes representing the corticofugal and corticocortical broad neuron classes. In mice, corticospinal and related subcerebral projection neurons are born during mid-corticogenesis (peak at embryonic day (E) 13.5), reside in layer V, project to brainstem and spinal cord, have large soma size, and extend large dendritic arbors with specific branching patterns and apical tufts reaching layer I. Callosal and related corticocortical projection neurons are born mostly after E14.5, predominantly populate the superficial layers II-III, project within the cortex, and have smaller soma and dendritic arbors than corticospinal projection neurons, but higher dendritic spine dynamics.[8–14]

FEZ family zinc finger 2 (*Fezf2*) is a transcriptional regulator and selector gene required for specification of corticospinal

 © 2024 The Authors. Published by Elsevier Inc.
This is an open access article under the CC BY-NC license (http://creativecommons.org/licenses/by-nc/4.0/).

and other corticofugal projection neuron subtypes, and repression of corticocortical projection neuron identity.[15–21] *Fezf2* controls multiple aspects of corticofugal neuron identity, including the use of glutamate as neurotransmitter, axonal projection via regulation of guidance molecules such as ephrin-B receptor 1 (EphB1),[15] and is required for normal dendritic morphology.[17] However, despite powerful and fruitful analyses of *Fezf2* transcriptional targets,[15] the molecular mechanisms whereby *Fezf2* controls dendritic development in corticofugal neurons have remained elusive. Here, we provide evidence for the role of a microRNA (miRNA) cluster downstream of *Fezf2* that serves as a link between projection neuron fate and dendritic morphology by regulating a signaling pathway controlling dendritic development in a neuron subtype-specific manner.

miRNAs are small non-coding RNAs that cooperatively repress multiple specific target genes post-transcriptionally.[22] miRNAs regulate molecular programs that refine neuron identity.[23–28] We previously identified a set of miRNAs selectively expressed by corticospinal vs. callosal projection neurons during development and that control cortical projection neuron fate.[29] Here, we show that the miR-193b∼365 microcluster: (1) is differentially expressed by developing corticospinal vs. callosal projection neurons, (2) is downstream of the selector gene *Fezf2*, (3) represses the callosal projection neuron-enriched signaling protein mitogen-activated protein kinase 8 (MAPK8, also known as JNK1), and (4) differentially controls dendritic morphology in deep-layer and superficial-layer neurons. Thus, regulation of MAPK8 signaling via expression of miR-193b∼365 cluster contributes to the development of dendritic arbors appropriate for corticospinal projection neurons, providing a mechanism that coordinates projection neuron identity, specified by *Fezf2*, and neuron-specific dendritic morphology.

RESULTS

The miR-193b∼365 cluster is enriched in corticospinal projection neurons and is downstream of the selector gene *Fezf2*

We have previously shown that miRNAs are differentially expressed by corticospinal vs. callosal projection neurons during their development and examined the genomic organization of corticospinal projection neuron-enriched miRNAs.[29] We identified that corticospinal projection neuron-enriched miRNAs mapped to two clusters: the 12qF1 miRNA cluster on mouse chromosome 12, which we previously studied and validated,[24,29] and the miR-193b∼365 miRNA cluster on mouse chromosome 16, the focus of this study. We first confirmed the specificity of the miR-193b∼365 cluster to corticospinal projection neurons in independent samples of purified corticospinal and callosal projection neurons on postnatal day (P) 2, and compared the relative quantity (RQ) of miRNA in corticospinal relative to callosal projection neurons via qPCR. We found that miR-193b is 2.9-fold enriched and miR-365 is 2.2-fold enriched in corticospinal vs. callosal projection neurons (Figure 1A). To begin to understand how the expression of the miR-193b∼365 cluster is regulated in these neuron subtypes, we carried out ATAC-seq in purified corticospinal and callosal projection neurons from P2 cortices. We found that whereas the putative promoter region upstream of the miR-193b∼365 cluster is accessible in callosal projection neurons, it is inaccessible in corticospinal projection neurons (Figure 1B). Interestingly, ENCODE identifies enhancers and promoter sequences in this region (Figure 1B). Since *Fezf2* is essential for specification of corticospinal projection neurons, but not for specification of callosal projection neurons, we compared this putative regulatory region to the *Fezf2* chromatin immunoprecipitation sequencing (ChIP-seq) dataset from Lodato and colleagues obtained from cortical progenitors transfected with a *Fezf2* expression construct, and therefore, differentiating into corticospinal and other corticofugal neuron types.[15] We found that the putative promoter/enhancer upstream of miR-193b∼365 and inaccessible in corticospinal projection neurons overlaps with a *Fezf2* chromatin binding footprint from the Lodato et al., dataset. This suggests that *Fezf2* may bind this regulatory region in differentiating corticospinal neurons, and that selective expression of the miR-193b∼365 cluster by corticospinal, but not callosal, projection neurons is controlled by *Fezf2* (Figure 1B). To analyze FEZF2 binding to this putative regulatory region upstream of miR-193b∼365, we expressed FEZF2-HA in the cortex and performed FEZF2-HA ChIP-qPCR in corticospinal and callosal neurons at P2. Compared with non-specific IgG pull-down, ChIP with anti-HA antibody from corticospinal neurons (CSMN FEZF2-ChIP) was enriched in five loci located in the putative regulatory region upstream of the miR-193b∼365 cluster, indicating binding of FEZF2 protein to this region (Figure 1B; 6.2-fold, 8.3-fold, 2.6-fold, 7.6-fold, and 4.6-fold enrichment FEZF2-ChIP qPCR in CSMN). However, FEZF2-ChIP from callosal neurons produced no enrichment, and therefore no indication of FEZF2 binding to this region upstream of miR-193b∼365 cluster in callosal neurons (Figure 1B, CPN FEZF2-ChIP).

To confirm that *Fezf2* regulates expression of the miR-193b∼365 cluster we transfected N2A mouse neuroblast cells with either *Fezf2* or control expression constructs and measured miR-193b and miR-365 expression by qPCR. We found that N2A cells significantly upregulated expression of miR-193b and miR-365 after transfection with *Fezf2* compared to control transfections (Figure 1C; miR-193b 4.81-fold upregulation; miR-365 2.53-fold upregulation). Also, we performed *Fezf2* knock-down experiments in neuron cultures obtained from E14 cortices and measured the levels of miR-193b and miR-365. We first confirmed the efficiency of *Fezf2* shRNA in culture our culture conditions (Figure S1A). We found downregulation of both miRs upon *Fezf2* shRNA transfection (Figure 1D; miR-193b 0.58-fold downregulation; miR-365 0.46-fold upregulation) Together, these results indicate that the miR-193b∼365 cluster is enriched in corticospinal vs. callosal projection neurons and that its expression is positively regulated by *Fezf2*.

miRs-193b and -365 control MAPK8 signal during neuron projection development

We carried out bioinformatic analyses to identify predicted targets of miRs-193b and 365 using miRanda,[30–33] Targetscan,[34–38] DIANALAB,[39–41] and miRDB.[42,43] Gene Ontology (GO) analysis of these predicted targets indicates that neuron development and neuron projection development are among the top ten over-represented biological processes for both

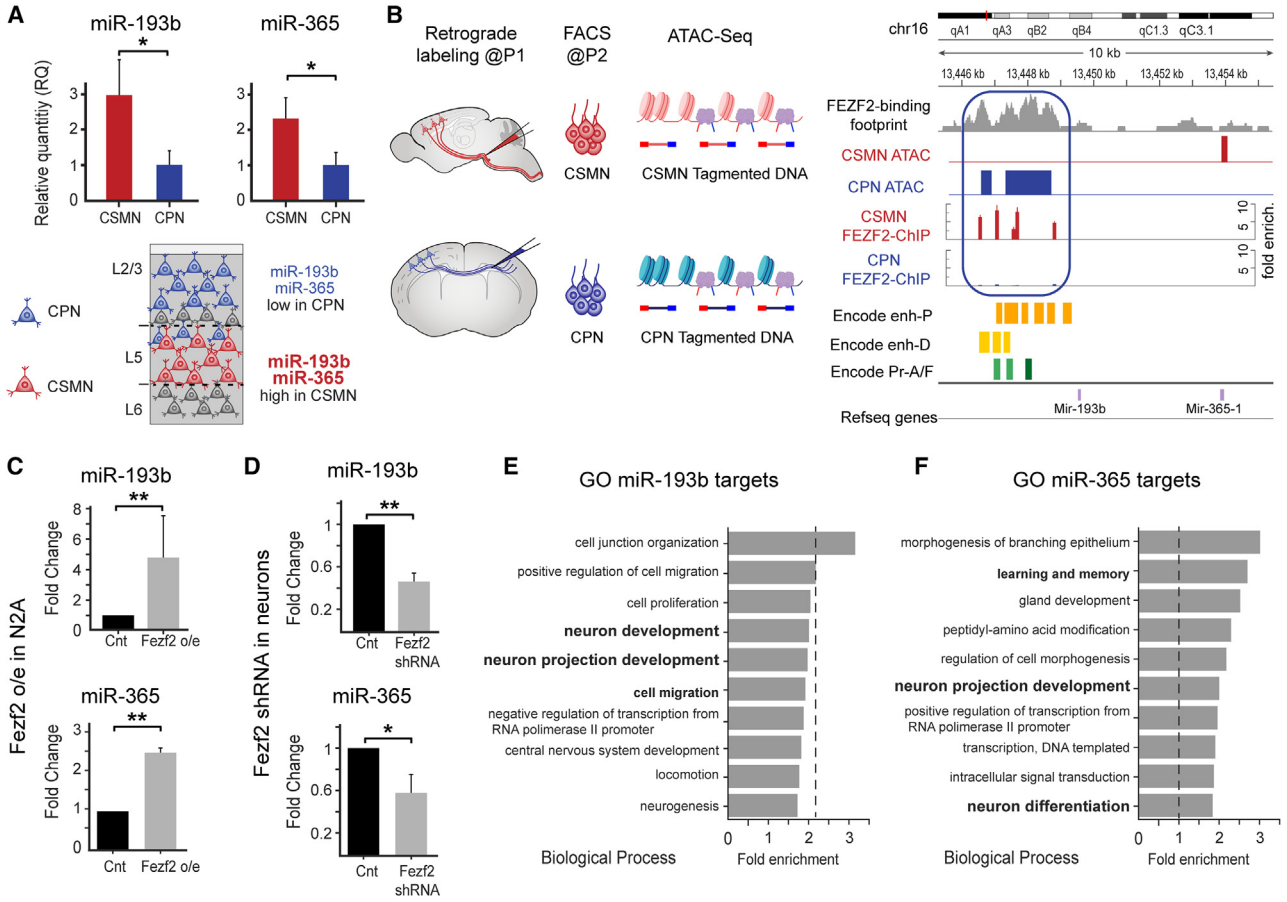

Figure 1. Expression of miR-193b∼miR-365 is enriched in CSMN and regulated by selector gene *Fezf2*

(A) Fold-enriched of miR-193B and miR-365 in corticospinal motor neurons (CSMN) vs. callosal projection neurons (CPN) at P2 (n = 3). Bottom panel, schematic summary of expression.

(B) ATAC-seq in CSMN vs. CPN. Left panel: experimental approach. Right panel: FEZF2 binding footprint from a study by Lodato et al.[15] (gray), CSMN-ATAC-seq (red), CPN-ATAC-seq (blue), CSMN FEZF2-HA ChIP-qPCR (red), CPN FEZF2-HA ChIP-qPCR (blue), ENCODE proximal enhancer (enh-P; orange), ENCODE distal enhancer (enh-D; yellow), ENCODE promoter active/flaking promoter (Pr-A/F; green). Boxed area marks a putative promoter/enhancer upstream of miR-193b-365, where FEZF2 footprint from the study by Lodato et al.[15] aligns with an inaccessible chromatin region in CSMN but accessible in CPN, and with FEZF2-HA ChIP-qPCR enriched loci in CSMN but not in CPN.

(C) Expression of miR193b and miR-365 by qPCR in *Fezf2* expressing N2A cells relative to control (n = 3), and (D) in *Fezf2* shRNA treated neuron cultures relative controls (n = 3).

(E and F) Top 10 over-represented biological processes by GO analysis of predicted targets of miR-193b (E) and miR-365 (F). Data are represented as mean ± SEM. Two-tail unpaired t test, p values are presented as follows; *$p < 0.05$, **$p < 0.01$. See also Figure S1.

miR-193b and miR-365 (Figures 1E and 1F). Other important processes relevant to cortical development and regulated by either miR-193b or miR-365 include cell migration, regulation of cell morphogenesis, neurogenesis, and learning and memory. Bioinformatic target analyses consistently predicted that both miR-193b and miR-365 target the signaling molecule *MapK8* (Figure 2A). Clustered miRNAs often cooperatively repress the same gene and/or interacting genes within a pathway.[44] Since our bioinformatic analyses predicted only a small number of shared individual targets (Table S1), and *MapK8* is required for cortical projection neuron development, we began our in-depth analyses of miR-193b∼365 targets with *MapK8*.

During neural development, *MapK8* controls multiple processes including cell death, proliferation, soma size, migration, and dendritic arborization.[45,46] Expression of *Mapk8* mRNA is high during brain development,[46,47] and in the cortex, it is preferentially expressed by callosal vs. corticospinal projection neurons during embryonic and early postnatal development[48,49] (Figures S1B and S1C), as would be predicted if miRs-193b and -365 were repressing *MapK8* in corticospinal but not callosal projection neurons. By P14, MAPK8 protein expression is highly enriched in layer II-III (predominantly callosal projection neurons with no corticospinal projection neurons) compared to layer V (predominantly corticospinal projection neurons), as would be predicted if miRs-193b and -365 were repressing its expression in corticospinal and other corticofugal projection neurons (Figures S1D and S1E). To investigate whether miRs-193b and -365 repress MAPK8 expression via the predicted sites in the

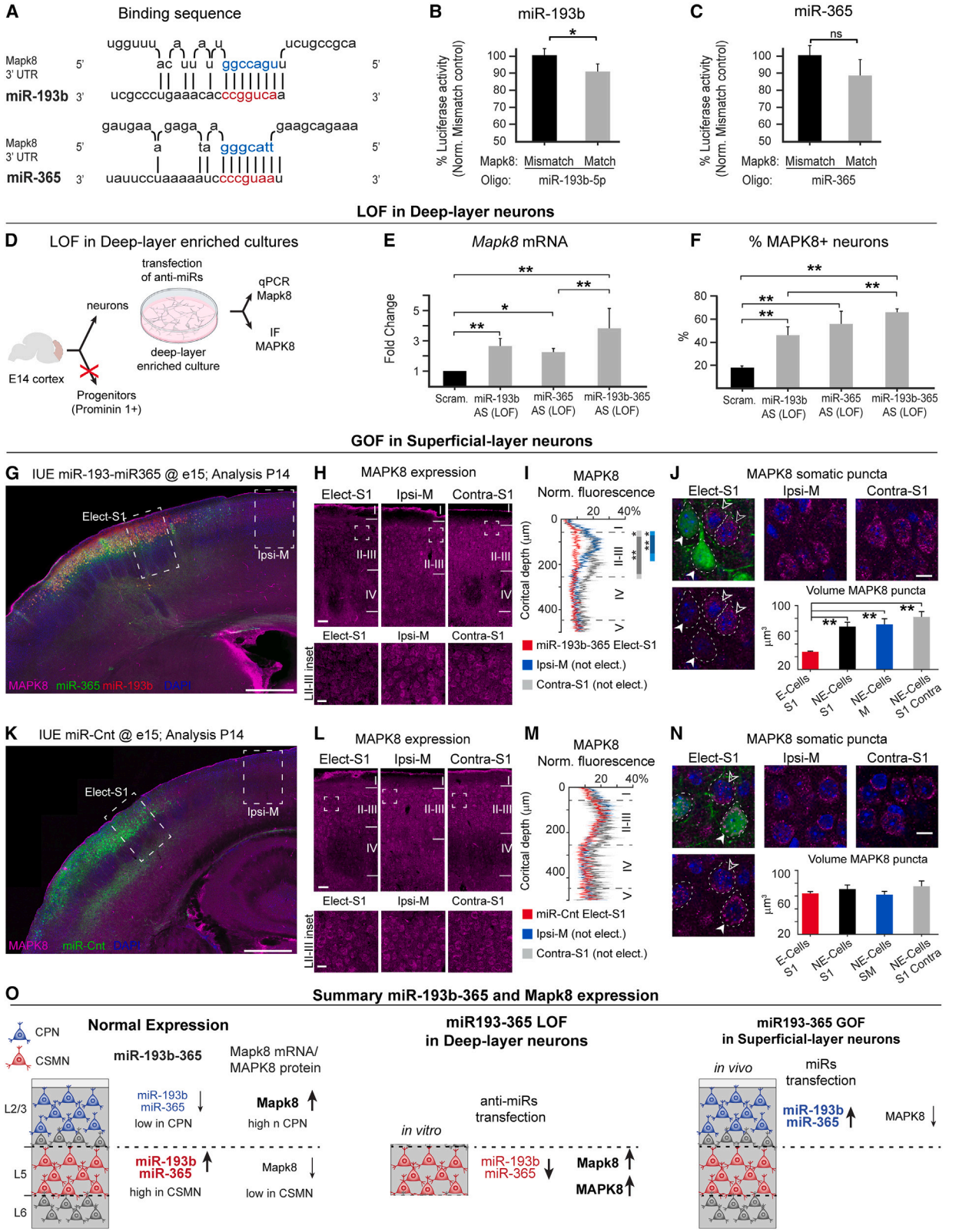

(legend on next page)

3′UTR, we performed luciferase reporter gene assays in COS7 cells, as previously described.[29,50,51] We used *MapK8* reporter vectors containing either wild-type or mutated (mismatch) target sites and their flanking 3′UTR sequences. We found that miR-193b oligonucleotides significantly repress *MapK8* luciferase reporter gene expression with wild-type, but not mismatch, miR-193b target sequences (Figure 2B). We found that miR-365 oligonucleotides also decreased MapK8 luciferase reporter gene expression with wild-type but not mismatched miR-365 target sequences, although this result did not reach statistical significance (Figure 2C). Scrambled control miRNA oligonucleotides did not repress the MapK8 luciferase reporter gene.

To test whether this finding extends to endogenous *Mapk8* mRNA and protein expression in mouse cortical neurons, we first performed loss-of-function (LoF) experiments in neuron cultures enriched in corticospinal and other corticofugal projection neuron subtypes (Figures 2D–2F). Cultures were obtained from E14 cortices, therefore before any significant production of superficial-layer neurons, and devoid of progenitors via exclusion of prominin 1-expressing cells. We then used lentiviral constructs to express antisense miR-193b-GFP (miR-193b-AS), antisense miR-365-GFP (miR-365-AS), and scrambled miRNA-GFP. We examined *Mapk8* mRNA via qPCR and MAPK8 protein expression by immunolabeling (Figure 2D). Transfection of antisense miR-193b and antisense miR-365 resulted in significant increase in *Mapk8* expression compared to scrambled control (Figure 2E; miR-193b-AS 2.64-fold upregulation, miR-365-AS 1.86-fold upregulation). Combined expression of both antisense constructs also resulted in increased *Mapk8* expression compared to scrambled controls and compared to antisense miR-365 (Figure 2E; miR-193b-365-AS 3.85-fold upregulation). Immunolabeling for MAPK8 and GFP reveals an increase in the number of MAPK8+ neurons in cultures transfected with antisense miR-193b and antisense miR-365 compared to control cultures transfected with scrambled-miRNA (Figure 2F; Scram controls 17%, miR-193b-AS 46%, miR-365-AS 56%). The number of MAPK8+ neurons in cultures transfected with both antisense miR constructs was also increased compared to scramble controls, and significantly increased compared to antisense miR-193b (Figure 2F, miR-193b-365-AS 67%). Together, these results indicate that miRs-193b and -365 downregulate *Mapk8* mRNA and protein expression, and suggest that the effect of combined miR-193b∼365 LoF is stronger than the effect of single miR LoF.

Next, we performed *in vivo* gain-of-function (GoF) experiments to test whether miR-193b and miR-365 overexpression reduces expression of MAPK8 by layer II-III neurons (predominantly callosal projection neurons). Layer II-III neurons normally do not express the miR-193b∼365 cluster, and express *Mapk8* mRNA and MAPK8 protein at a high level compared to corticospinal projection neurons and other neurons in layer V (Figures S1B–S1D). To express miR193b, miR-365, miR193b-miR-365, or scrambled control miRNAs in callosal projection neurons, we performed *in utero* electroporation (IUE) at E15, targeting the somatosensory cortex. For miR193b-miR-365 GoF experiments, we confirmed that co-electroporated miR193b-miR-365 constructs were co-expressed in neurons (Figure S2A). We quantified the overall MAPK8 immunofluorescence signal intensity, which includes the signal from somata and neuropil, in miR-electroporated and control-electroporated primary somatosensory areas (S1-area) at P14. As additional internal controls, we analyzed MAPK8 signal in the non-electroporated contralateral S1-area (Contra-S1), and the non-electroporated motor area (Ipsi-M) adjacent to the electroporated S1-area. We found that the combined overexpression of miR193b-miR-365 strongly reduces MAPK8 in layer II-III of the electroporated S1-area compared to non-electroporated Ipsi-M or Contra-S1 areas (Figures 2G–2I). This reduction was not observed with electroporation of scrambled control constructs (Figures 2K–2M).

In addition to the analysis of the overall signal intensity, we analyzed MAPK8 signal at the cellular level, quantifying the volume of MAPK8+ puncta in somata. This is because *Mapk8* regulation via miRNAs has been demonstrated in different cell compartments, and likely contributes to the spatial compartmentalization of MAPK8 functions in different cell types.[46,52–54] Therefore, the effects of miR193b and miR-365 on MAPK8 expression may differ in the soma and neuropil. Within the

Figure 2. miR-193b and miR-365 repress MapK8 *in vitro* and *in vivo*

(A) Alignments of seed sequences (red) of miR-193b and miR-365 to target sequences in the MapK8 3′ UTR (blue).

(B) miR-193b oligonucleotides repress a MapK8 3′UTR luciferase reporter gene bearing wild-type, but not mismatch, target sequences in COS cells ($n = 3$, two-tail unpaired t test, p values are presented as follows; $^{*}p < 0.05$).

(C) miR-365 oligonucleotides reduced luciferase activity from a MapK8 3′UTR luciferase reporter gene bearing wild-type but not reaching statistical significance in COS cells ($n = 3$, two-tail unpaired t test).

(D–F) miRs loss-of-function (LoF) in deep-layer neuron cultures. (D) Experimental approach. (E) *Mapk8* mRNA expression by qPCR in miR-193b AS, miR-365 AS, and miR-193b-365 AS antisense miRs constructs, ($n = 3$, ANOVA-Tukey, p values are presented as follows; $^{*}p < 0.05$, $^{**}p < 0.01$). (F) Percent of MAPK8+ in miR-193b AS, miR-365 AS, and miR-193b-365 AS antisense miRs constructs, ($n = 3$, ANOVA-Tukey, p values are presented as follows; $^{*}p < 0.05$, $^{**}p < 0.01$).

(G–N) miRs gain of function (GoF) in superficial-layer neuron *in vivo*. (G, and K) Coronal sections of P14 brain electroporated at E15 with miR-193b (red) and miR-365 (green) in (G), and with miR-Scrambled control constructs (green) in (K), immunolabeled for MAPK8 (magenta). (H and L) MAPK8 immunolabeling. Left, expression in the electroporated primary somatosensory area (Elect-S1). Center and left, expression in two non-electroporated areas: Motor cortex ipsilateral to the electroporation (Ipsi-Motor), and somatosensory cortex contralateral to the electroporation (Contra-S1). Boxed areas in layer II-III are shown at higher magnification in insets. (I and M) Quantification of fluorescence intensity of MAPK8 signal from layer I (LI) to the superficial part of LV, in Electr-S1 (red), Ipsi-M (blue), and Contra-S1 (gray) areas. (J and N) Images and quantification of MAPK8 immunofluorescence in somatic puncta. Quantification in electroporated neurons (E-Cells S1) and adjacent non-electroporated neurons (NE-Cells S1) in the somatosensory cortex, non-electroporated neurons in motor cortex (NE-Cells M), and non-electroporated neurons in the somatosensory area contralateral to the electroporation (NE-Cells S1 Contra). (I, J, M, and N) ANOVA-Tukey, p values are presented as follows; $^{*}p < 0.05$, $^{**}p < 0.01$. $n = 5$ for miR-193b-miR-365 electroporation; $n = 4$ for miR-Cnt.

(O) Summary of miR-193b-365, *Mapk8* mRNA, and MAPK8 in control superficial and deep cortical neurons, and after miR-193b-365 LoF and GoF. Data are represented as mean ± SEM. Scale bars, 500 μm (G and K), 50 μm (H and L), 20 μm (H and L insets), 10 μm (J and N). See also Figures S1 and S2.

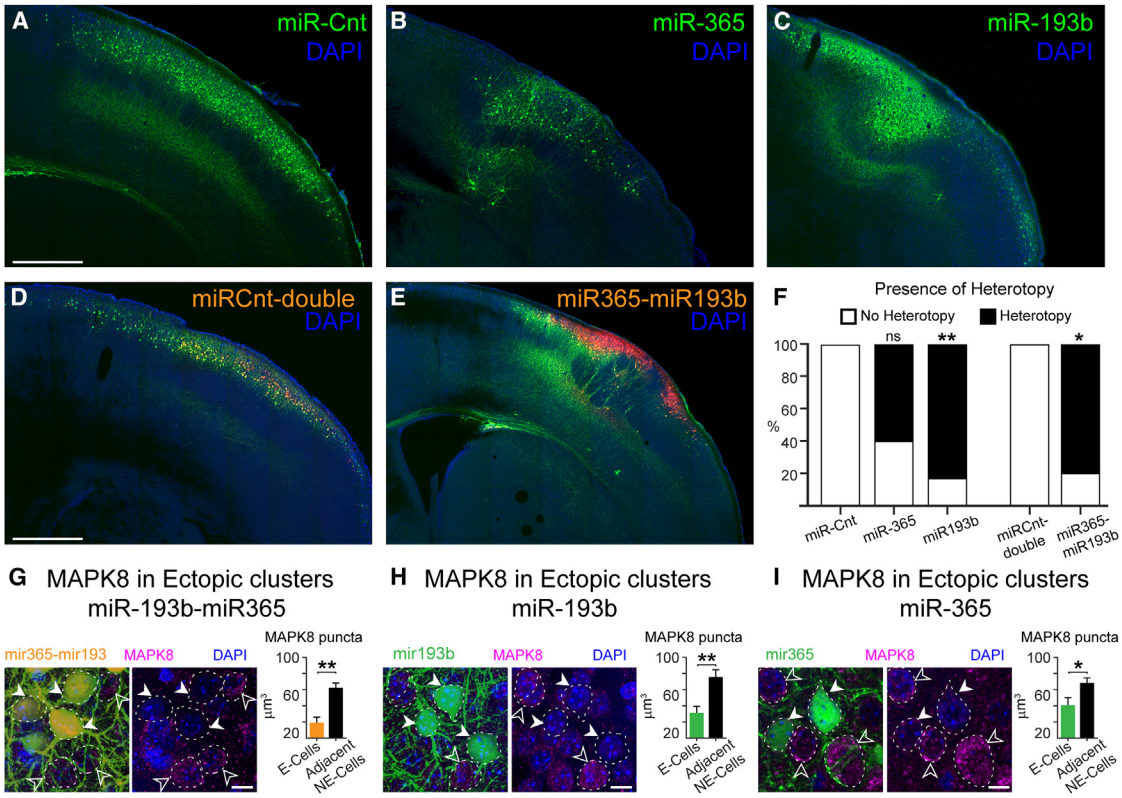

Figure 3. miR-193b and miR-365 expression in superficial-layer neurons alters their migration

(A–E) Coronal sections of P14 brain electroporated at E15 with single miR-scramble sequence (miR-Cnt), miR-365, miR-193b, co-electroporation of miR-scramble sequences of miR-193b and miR-365 (miR-Cnt-double), and co-electroporation of miR-193b and miR-365 (miR-193b-miR-365).

(F) Quantification of brains with heterotopies per condition. Brain per condition, $n = 4$ miR-Cnt, $n = 6$ for miR193b, $n = 5$ miR-365, miR-Cnt-double $n = 4$, miR-193b-miR-365 $n = 5$. Fisher-exact test, p values are presented as follows; $^{*}p < 0.05$, $^{**}p < 0.01$.

(G–I) Images and quantification of MAPK8 immunofluorescence of somatic puncta in electroporated neurons (E-Cells) and adjacent non-electroporated neurons (NE-Cells) of ectopic clusters in the primary somatosensory cortex after expression of either miR-193b-miR-365 (G), miR-193b (H), or miR-365 (I). t test, p values are presented as follows; $^{*}p < 0.05$, $^{**}p < 0.01$. Data are represented as mean ± SEM. Scale bars, 500 µm (A–E), 10 µm (G–I). See also Figure S3.

electroporated S1-area, layer II-III neurons expressing both miRs-193b and -365 showed reduced MAPK8 somatic signal compared to adjacent non-electroporated neurons. Also, layer II-III neurons expressing both miR-193b-365 in S1 showed decreased MAPK8 compared to non-electroporated layer II-III neurons in either Contra-S1 or Ipsi-M areas (Figure 2J). This decrease was not found in layer II-III neurons electroporated with scrambled control constructs (Figure 2N).

Next, we analyzed whether GoF of each miRNA independently reduces MAPK8 signal *in vivo*. We found that expression of miR-193b significantly reduces the overall MAPK8 signal in the layer II-III of the electroporated S1-area compared to Ipsi-M or Contra-S1, and MAPK8 signal in the somata of electroporated neurons (Figures S2B–S2E). Expression of miR-365 did not significantly change the overall MAPK8 signal in layer II-III (Figures S2F–S2H); however, at the cellular level, it reduced MAPK8 signal in the somata (Figure S2I). These results indicate that MAPK8 signal in somata is reduced by either miR, whereas MAPK8 signal in the neuropil might be preferentially regulated by miR-193b. Overall, miRs-193b-365 LoF in deep-layer neuron cultures results in increased MAPK8 signal, and miRs-193b-365 GoF in superficial-layer neurons results in decreased MAPK8 signal (Figure 2O).

MAPK8 regulates cell migration,[46,47] which is among the top biological processes detected by our GO analysis as regulated by the miR-193b∼365 cluster (Figure 1). To confirm that regulation of MAPK8 signal via miR-193b∼365 is important for neuron development, we analyzed whether the decrease in MAPK8 observed after miR-193b∼365 expression affects neuron migration. After IUE at E15 of miR193b, miR-365, both miR193b and miR-365, or scrambled miRNA, we analyzed the presence of heterotopic clusters of neurons that failed to migrate into the superficial layers at P14. We found a significantly increased percentage of brains with clusters of heterotopic neurons in the deep layers or the white matter after electroporation of miR-193b alone and miRs-193b and -365 compared to scrambled controls (heterotopy+ brains: 83.3% miR-193b, 80% miR-193b-miR-365; 0% scrambled-miRNA; Figures 3A–3F). The percentage of brains with heterotopic clusters after electroporation of miR-365 was higher than in controls; however, this difference did not reach statistical significance (heterotopy+ brains: 60% miR-365; 0% scrambled control; Figures 3B and 3F). We

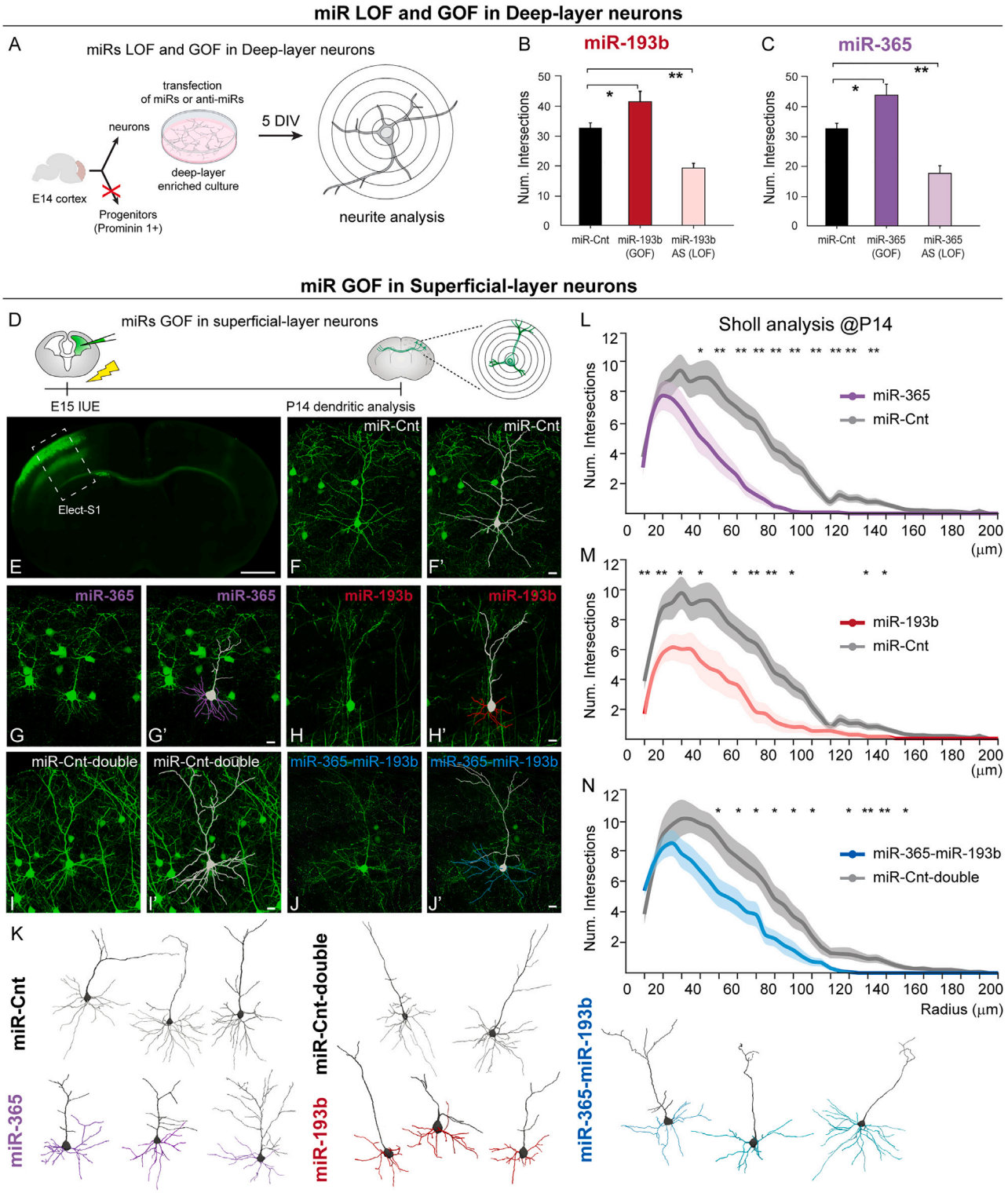

Figure 4. miR-193b and miR-365 gain-of-function decreases dendritic complexity in superficial-layer neurons

(A) Experimental approach for miRs loss-of-function (LoF) and gain-of-function (GoF) in deep-layer neuron cultures.

(B and C) Analysis of neurite branching by Sholl analysis after miR-193b GoF and LoF (B), and after miR-365 193b GoF and LoF. ANOVA-Tukey, *p* values are presented as follows; $*p < 0.05$, $**p < 0.01$ ($n = 3$ per condition).

(D) Experimental approach for *in vivo* miRs GoF in superficial-layer neurons.

(legend continued on next page)

confirmed that neurons in the heterotopic clusters have reduced MAPK8 signal compared to non-electroporated nearby/adjacent neurons, as we previously showed in miR-193b and -365 electroporated layer II-III neurons (Figures 3G–3I). These data confirm the importance of the miR-193b∼365 cluster for cortical projection neuron development and suggest that, within the cluster, miR-193b primarily contributes to controlling neuron migration via regulation of MAPK8 protein level.

Interestingly, it has been previously shown that *Fezf2* overexpression in superficial-layer neurons alters their differentiation and migration, creating ectopic clusters of superficial-layer neurons in the deep layers and white matter.[16,55] The observation of a common migration phenotype after *Fezf2* or miR-193b-miR365 cluster overexpression in layer II-III neurons further supports our results revealing *Fezf2* regulation of the miR-193b∼365 cluster, and is consistent with the interpretation that the migration defects previously observed after *Fezf2* overexpression may be mediated by dysregulation of MAPK8 signal via abnormal upregulation of the miR-193b∼365. To further investigate the link between *Fezf2*, miR-193b∼365 cluster, and *Mapk8*, we measured *Mapk8* mRNA in N2A cells after *Fezf2* overexpression. We observed decreased expression of *Mapk8* mRNA upon *Fezf2* overexpression (Figure S3A). This is consistent with our previous results showing upregulation of miR-193b and miR-365 in this condition. Overall, our data support the conclusion that *Fezf2* regulates the expression of miR-193b-365 microcluster, which in turn represses MAPK8.

miRs-193b and -365 control dendritic morphology in a neuron subtype-specific manner

Layer II-III and layer V neurons have dendrites with distinct characteristics, including field size, morphology, and spine density.[8,10–13] MAPK8 is a key regulator of neurite branching, dendritic morphology, and spine dynamics.[45,46,56–59] *Mapk8* is differentially expressed in layer II-III and layer V neurons,[48,49] and its loss of function has different effects on the dendrites of these neuron types.[57] Therefore, we reasoned that MAPK8 signal must be differentially controlled in layer II-III and layer V neurons. Since MAPK8 is regulated by the miR-193b∼365 cluster, which is differentially expressed by corticospinal vs. callosal projection neurons, we posited that miR-193b∼365 may control neurite outgrowth and dendritic branching in a neuron subtype-specific manner via differential regulation of MAPK8. In this way, the miR-193b∼365 cluster may contribute to the distinct development of dendritic fields of these neuron subtypes.

To test this hypothesis, we first carried out miR-193b∼365 cluster GoF and LoF experiments in cultures enriched in corticospinal and other deep-layer neurons and evaluated neurite branching (Figures 4A–4C). We transfected miR-193b or miR-365 for GoF experiments, and antisense miRs, miR-193b-AS or miR-365-AS for LoF experiments. Neurite branching was examined after 5 days in culture via Sholl analysis. We found that GoF of either miR-193b or miR-365 results in a significant increase in neurite branching compared to scrambled controls, whereas either miR-193b or miR-365 LoF results in a significant decrease in neurite branching compared to scrambled controls (Figures 4B and 4C). These results indicate that high expression of the miR-193b∼365 cluster promotes neurite branching in cultures enriched for deep-layer cortical neurons. Together with our previous experiments showing that miR-193b∼365 LoF resulted in increased *Mapk8* mRNA and protein in deep-layer neurons (Figures 2E and 2F), our results indicate that high expression of the miR-193b∼365 downregulates MAPK8 signaling, which in deep-layer neurons promotes neurite branching. This conclusion is further supported by previous *in vivo* work demonstrating increased dendritic branching in layer V neurons in *Mapk8 KO* mice.[57]

To further investigate whether miR-193b∼365 regulates dendritic morphology and branching in a neuron subtype-specific manner, we performed GoF experiments targeting superficial-layer neurons. After IUE of miR-193b, miR-365, miR-193b and miR-365, or scrambled controls at E15, we analyzed the complexity of the basal dendritic arbors of electroporated layer II-III neurons at P14 (Figure 4D). As shown earlier, MAPK8 is reduced in layer II-III miR-193b or -365 electroporated neurons (Figures 2J, S2E, and S2I). Expression of either miR-193b, miR-365, or both resulted in a significant decrease in the dendritic complexity and branching of the basal dendritic arbors of layer II-III neurons compared to scrambled controls (Figures 4E–4N). Importantly, these results are consistent with previous work demonstrating decreased dendritic branching by layer II-III neurons in *MapK8 KO* mice compared to wild-type.[57] Thus, miR-193b and -365 GoF in layer II-III results in decreased MAPK8 expression, which in this neuron type leads to decreased dendritic complexity.

Beyond dendritic branching, MAPK8 is also a key regulator of dendritic spine morphology, turnover, and motility.[45,58] These processes are essential to regulate synaptic input connectivity, which is controlled in a neuron-specific manner. Layer II-III and layer V neurons differ in spine density during development and in adults.[10,12,13] Previous work has shown that MAPK8 signal activation promotes spine retraction, while MAPK8 inhibition reduces spine elimination, in hippocampal neurons[45]; however, the effect of MAPK8 regulation in dendritic spines in cortical projection neurons has not been studied.

As a first step to understanding whether regulation of MAPK8 signal may affect dendritic spines in cortical neurons, we analyzed

(E) Representative image of the electroporated area analyzed in all conditions (Elect-S1).
(F–J′) Images of electroporated neurons for each condition: single miR-scramble sequence (miR-Cnt) (F and F′), miR-365 (G and G′), miR-193b (H and H′), co-electroporation of miR-scramble sequences of miR-193b and miR-365 (miR-Cnt-double) (I and I′), and co-electroporation of miR-193b-miR-365 (J and J′). For each condition, a representative neuron is shown with and without dendritic tracing.
(K) Examples of traced neurons for each condition. Only basal dendritic arbors were used for Sholl analysis (gray for miR-Cnt and miR-Cnt-double, magenta for miR-365, red for miR-193b, and cyan for miR-193b-miR-365).
(L–N) Analysis of dendritic complexity by Sholl analysis at P14. ANOVA-Tukey, p values are presented as follows; $^{*}p < 0.05$, $^{**}p < 0.01$. Reconstructed neurons n = 16 miR193b-miR-365, n = 14 miR-Cnt-double, n = 14 miR-365, n = 8 miR-193b, n = 18 miR-Cnt. Data are represented as mean ± SEM. Scale bars, 500 μm (E), 15 μm (F–J′). See also Figure S3.

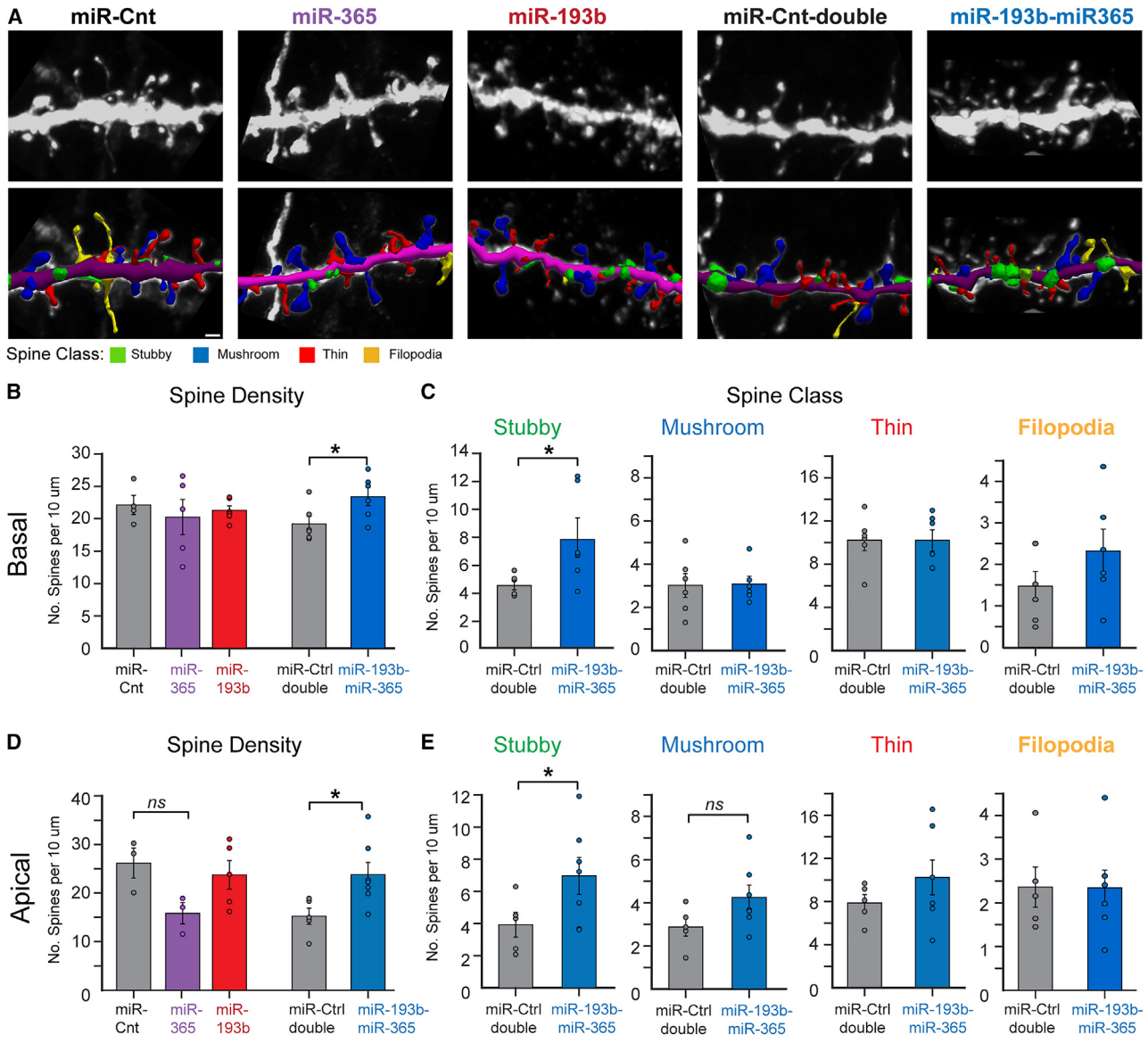

Figure 5. miR-193b and miR-365 cooperatively regulate spine density

(A) Dendritic segments of neurons expressing single miR-scramble sequence (miR-Cnt), miR-365, miR-193b, miR-scramble sequences of miR-193b and miR-365 (miR-Cnt-double), or miR-193b-miR-365. For each condition, images are shown with (bottom) and without (top) reconstruction.

(B and C) Quantification in segments of basal dendrites. (B) Comparison of spine density across groups indicates increased density with miR-193b-miR-365 expression compared to corresponding control miR-Cnt-double. $n = 6$ segments from different neurons for miR-193b-miR-365, $n = 6$ miR-Cnt-double, ANOVA-Tukey. (C) Comparison of density for each spine class between miR-193b-miR-365 and miR-Cnt-double. One-tail unpaired t test, p values are presented as follows; $^*p < 0.05$.

(D and E) Spine quantification in segments of apical dendrites. (D) Spine density only increased with miR-193b-miR-365 expression with respect to miR-Cnt-double. $n = 7$ segments from different neurons for miR-193b-miR-365, $n = 5$ miR-Cnt-double, ANOVA-Tukey. (E) Only Stubby spines significantly increased after miR-193b-miR-365 expression with respect to miR-Cnt-double. One-tail unpaired t test, p values are presented as follows; $^*p < 0.05$. Data are represented as mean ± SEM. Scale bars, 0.5 μm.

if the reduction in MAPK8 signal observed in miR-193b and -365 electroporated layer II-III neurons affected spine density. Also, since spine morphology (class) is correlated to spine stability and synaptic maturity, we analyzed whether specific classes of spines were differentially affected by decreased MAPK8 signal after miR-193b or -365 expression. Spines are typically classified as mushroom, stubby, thin, or filopodial based on their morphology.[59,60] Mushroom and stubby spines are considered stable and mature, while thin and filopodial spines are more dynamic.[59,61–63] We found that neither miR-193b nor miR-365 alone had a significant effect on spine density in basal or apical dendrites compared to scrambled controls (Figures 5A, 5B, and 5D).

However, in neurons expressing both miR-193b and -365, there was a significant increase in spine density in basal and apical dendrites compared to scrambled controls (Figures 5B and 5D). When we analyzed spines by class, we found a significant increase in stubby spines in both apical and basal dendrites (Figures 5C and 5E). In apical dendrites, the density of mushroom spines was also increased, although this result did not reach statistical significance. These results showing an increase in spine density and bias toward stable spines after the reduction of MAPK8 signal induced by miR-193b∼365 overexpression suggest that this pathway may regulate spines in cortical neurons, in addition to dendritic branching. Our results are consistent with previous studies of spine dynamics in hippocampal neuron cultures indicating that inhibition of MAPK8 signaling reduces spine elimination and activation of MAPK8 signaling promotes spine retraction,[45] with the caveat that our studies only provide a static snapshot of the state of spines. Thus, while either miR-193b or miR-365 regulate dendritic branching, only the combined effect of both miR-193b-365 might alter dendritic spines in ways that resemble the effects of reduced MAPK8 *in vivo*.

Collectively, these results from GoF experiments in layer II-III neurons and GoF/LoF in deep-layer neurons indicate that the miR-193b∼365 cluster differentially regulates the development and branching of dendritic arbors in superficial-layer and deep-layer neurons via control of MAPK8 signaling in these neuron classes.

DISCUSSION

The mechanisms that coordinate the emergence of the distinct characteristics defining a neuron type are unknown. In particular, the molecular mechanisms of dendritic development in specific cortical projection neuron subtypes represent the least understood aspect of cortical projection neuron development. Here, we identify a mechanism linking the regulation of dendritic development and morphology with neuron identity in corticospinal projection neurons, a clinically important and prototypical subtype of corticofugal projection neuron. We show that the miR-193b∼365 miRNA cluster is expressed under the control of corticofugal selector gene *Fezf2* and, in turn, via repression of MAPK8 signal, controls the development of dendritic arbors in corticospinal and other corticofugal projection neurons.

Previous work revealed that *Fezf2* is required for normal dendritic development in deep-layer pyramidal neurons,[17,64] and increases dendritic growth and complexity when overexpressed in non-pyramidal neuron types.[65] This work indicated a role for *Fezf2* in dendritic development and reinforced the notion that *Fezf2* broadly controls aspects of corticofugal neuron identity development.[15] However, the specific molecular pathways by which *Fezf2* regulates dendritic development have remained unexplored. Our work shows that the miR-193b–365 miRNA cluster is regulated by *Fezf2* and promotes dendritic branching in deep-layer neurons via regulation of MAPK8. This effect is neuron class-specific, since miR-193b and -365 overexpression in superficial layer corticocortical neurons reduces, rather than promotes, their dendritic complexity. Importantly, the effect of miR-193b and miR-365 expression in deep and superficial-layer neurons recapitulates the differential effect of loss of *Mapk8* function in layer V (increased branching) and in layer II-III neurons (decreased branching) described in *Mapk8* knockout mice.[57] Taken together, our approach combining miR-193b and miR-365 LoF and GoF, *in vitro* and *in vivo*, reveals that regulation of the MAPK8 signaling pathway, by miR-193b∼365, is an important mechanism by which *Fezf2* controls dendritic development in a neuron subtype-specific manner.

Dendritic growth and branching are precisely regulated during the development of each neuron type, as these processes determine the specific dendritic field size and architecture, and thus, the inputs each neuron type potentially receives. While corticospinal projection neurons and other layer V subcerebral projection neurons have large dendrites extending broad apical tufts in layer I, layer II-III neurons have smaller dendritic arbors that may or may not possess an elaborated apical tuft.[8,9,14,66] The regulation of MAPK8 via miR-193b∼365 revealed here is at least one way in which *Fezf2* may coordinate the formation of dendritic arbors with the size and architecture appropriate for neurons projecting to subcerebral targets.

Spine density and dynamics are key to determining the synaptic inputs each neuron receives.[60] Layer II-III and layer V neurons exhibit different spine densities and dynamics during postnatal maturation and in adults.[10,13] Spine formation is strongly regulated by activity during differentiation and maturation[59,60]; however, intrinsic neuron-specific mechanisms may also contribute to the distinct spine developmental dynamic characteristic of each neuron type. We show that miR-193b∼365 regulates MAPK8 signal, and decreased MAPK8 alters spine development in layer II-III neurons. This suggests that regulation of MAPK8 may have effects beyond the control of dendritic branching, and perhaps it may also play a role in fine-tuning spine development. However, whether reduced MAPK8 expression would have a similar effect in spines in other neuron types, and specifically, whether reduced MAPK8 regulated via miR-193b∼365 in layer V corticofugal neurons would regulate spines is an open question. Studies in *Mapk8* KO mice have shown that loss of MAPK8 differently affects distinct neuron types in the hippocampus. Loss of *Mapk8* alters the spine density and dynamics in CA3 pyramidal neurons but does not affect spines in CA1 neurons.[45,58] Our studies suggest the possibility that MAPK8 regulates spine development in cortical projection neurons and lay the foundation for future studies investigating the specific role of MAPK8 in spine development in different cortical neuron types, and of MAPK8 regulation via miR-193b∼365 in deep-layer neurons.

MAPK8 phosphorylates a wide range of nuclear and cytosolic substrates.[46] Nuclear MAPK8 regulates transcription factor activity and chromatin state.[67,68] Cytosolic MAPK8 regulates neuron polarization, migration, and axo-dendritic architecture during development, and plays important roles in spine growth, synaptic plasticity, and memory formation throughout life.[47] The spatial segregation of MAPK8 into different neuron subcellular compartments underlies its distinct functions.[46,56] *Mapk8* regulation via miRNAs has been demonstrated in different contexts and likely contributes to the spatial compartmentalization of MAPK8 functions.[46,52–54] miRNAs can control protein availability in somata, dendrites, axons, and spines and play critical roles in fate acquisition, dendritogenesis, spinogenesis, and

axon guidance.[23,25,69–71] In the cerebral cortex, expression of MAPK8 dominates in the neuropil compartment.[46] Our studies indicate that miR-193b∼365 regulates dendritic branching and spinogenesis, and suggest that miR-193b and miR-365 may have different effects on MAPK8 signal in somata and neuropil. Both miRs reduced MAPK8 signal in somas, however, miR-365 does not significantly reduce the overall MAPK8 signal in the superficial layers, which may suggest a weaker regulation of miR-365 in the neuropil. However, miR-365 is capable of regulating dendritic branching and is needed in combination with miR-193b to regulate spine density. Regulation of dendritic branching and spines may require different levels of MAPK8, and the optimal repression needed for appropriate spine regulation may require both miR-193b and miR-365. Future studies will further determine the specific requirements of each miR in these processes, but overall, our results are consistent with known cooperative repression mechanisms of miRNA action.[44,72]

Limitations of the study

Overall, our results using multiple approaches (i.e., *in vivo* GoF, *in vitro* GoF and LoF, multiple cell types) indicate that miR-193b∼365 cluster contributes to regulating dendritic development in specific cortical neuron types via regulation of MAPK8 signaling. While some isolated results did not reach statistical significance, they showed an effect consistent with the overall premise. This is likely due to intrinsic differences between the experimental systems used. For example, we observed no statistically significant downregulation of *Mapk8* by miR-365 in the luciferase reporter assay in COS cells; however, all our miR-365 LoF and GoF assays in neurons, *in vitro* and *in vivo*, showed significant effects on MAPK8. This highlights the robustness and importance of using multiple approaches, each with advantages and limitations.

The effect of miR-193b∼365 in the morphology of dendritic arbors in superficial and deep-layer neurons was performed using different approaches. Analysis of dendritic morphology after miR-193b∼365 GoF in superficial-layer neurons was performed *in vivo*, while dendritic analysis after miR-193b∼365 LoF in deep-layer neurons was performed *in vitro*. *In vivo* experiments allowed us to analyze the dendritic complexity in the context of intact cortical tissue, which requires dendritic arbor reconstruction. Dendritic arbor size imposes limitations on this type of morphological analysis. Large dendritic arbors, such as those of layer V neurons, typically cannot be entirely captured and reconstructed even in thick cortical sections. For dendritic analysis after miR-193b∼365 LoF in deep-layer neurons, we used an *in vitro* approach. Dendritic analysis in cultured neurons is routinely used to study regulation of dendritic growth and branching, as it allows dynamic visualization of entire dendritic arbors in the culture surface. Although dendritic morphology in cultured neurons may not entirely recapitulate the complexity of arbors in the brain tissue, this analysis allowed us to test the effect of miR-193b∼365 in dendritic branching and growth and to distinguish the effects of miR-193b∼365 LoF and GoF in the dendritic arbors of deep-layer neurons. Future studies could address this limitation by analyzing large cortical regions at high resolution to reconstruct layer V dendritic arbors under different miR and MAPK8 expression conditions.

Our studies did not explore whether miR-193b-miR-365 regulates MAPK8 function in axon guidance in corticospinal projection neurons and other corticofugal neurons. MAPK8 is required for netrin-1 signaling through DCC (DCC Netrin 1 receptor),[73] which is required during callosal projection guidance.[74] Indeed, the formation of the corpus callosum and anterior commissure is impaired in mice lacking the MAPK scaffold protein JASP1, required for MAPK8 function.[75] Future experiments, including examination of axonal projections, will be important to determine whether the corticospinal projection neuron-expressed miR-193b and miR-365 cooperatively repress this callosal-expressed netrin-1 attractive midline crossing axon guidance pathway in developing corticospinal projection neurons, via MAPK8 repression.

RESOURCE AVAILABILITY

Lead contact

Further information and requests for resources and reagents should be directed to and will be fulfilled by the lead contact, Dr. Maria J. Galazo (mgalazo@tulane.edu).

Materials availability

All unique/stable reagents generated in this study are available with a materials transfer agreement from the lead contact for academic, non-commercial use; negotiation and completion of a materials transfer agreement with Tulane University and Stanford University is required if there is potential for commercial application.

Data and code availability

- The DOIs of key resources are listed in the key resources table. Other data reported on this paper will be shared by the lead contact upon request.
- This paper does not report original code.
- Any additional information required to reanalyze the data reported in this paper is available from the lead contact upon request.

ACKNOWLEDGMENTS

We thank members of the S.T. and M.J.G. labs. Work supported by grants from NIH (K08 NS091531), AOSpine North America (Young Investigator Research Grant Award), Stanford McCormick Faculty Award, Stanford Maternal and Child Health Research Institute Pilot Award, Stanford Maternal and Child Health Bridge Funds award, and a Curci Foundation award to S.T. M.J.G. is supported by grants from NIH (R01 NS128106), Louisiana Board of Regents (LEQSF(2021-24)-RD-A-14)), Brain and Behavior Foundation NARSAD Young Investigator Award (BBF 27329), and Carol Lavin Bernick Faculty Grant. S.T. is a Tashia and John Morgridge Endowed Faculty Scholar in Pediatric Translational Medicine of the Stanford Maternal and Child Health Research Institute. M.J.G. is the Stepping Stone Foundation Early Career Professor in Cell and Molecular Biology at Tulane University. We acknowledge the Stanford Neuroscience Microscopy Service, supported by NIH NS069375, and Tulane Brain Institute microscopy core, supported by Louisiana Board of Regents Enhancement Grant LEQSF(2018-23)-ENH-DE-15.

AUTHOR CONTRIBUTIONS

Research designed by S.T., M.J.G., A.I., V.B.S., and L.O.V.; research performed by A.I., L.O.V., V.B.S., R.K.C., A.T., M.A., R.N., V.L., S.T., and M.J.G.; data analysis by A.I., L.O.V., V.B.S., R.K.C., S.T., and M.J.G.; manuscript written by A.I., L.O.V., S.T., and M.J.G. M.J.G. and S.T. are co-seniors. M.J.G. is the corresponding author.

DECLARATION OF INTERESTS

The authors declare no competing interests.

STAR★METHODS

Detailed methods are provided in the online version of this paper and include the following:

- KEY RESOURCES TABLE
- EXPERIMENTAL MODEL AND STUDY PARTICIPANT DETAILS
  - Cell lines
  - Mouse lines
- METHOD DETAILS
  - Corticospinal projection neuron and callosal projection neuron FACS-purification
  - RNA purification
  - ATAC-seq library preparation and sequencing
  - ATAC-seq analysis
  - miRNA target prediction and Gene Ontology (GO) analysis
  - Quantitative PCR (qPCR)
  - ChiP-qPCR
  - Luciferase assays
  - Lentivirus vectors
  - Cell culture
  - Immunocytochemistry of cultured cells
  - Sholl analysis
  - *In utero* electroporation
  - Immunocytochemistry of brain sections
  - Microscopy and image analysis
- QUANTIFICATION AND STATISTICAL ANALYSIS

SUPPLEMENTAL INFORMATION

Supplemental information can be found online at https://doi.org/10.1016/j.isci.2024.111500.

Received: January 16, 2024
Revised: July 30, 2024
Accepted: November 26, 2024
Published: November 28, 2024

REFERENCES

1. Angevine, J.B., and Sidman, R.L. (1961). Autoradiographic study of cell migration during histogenesis of cerebral cortex in the mouse. Nature *192*, 766–768.
2. Greig, L.C., Woodworth, M.B., Galazo, M.J., Padmanabhan, H., and Macklis, J.D. (2013). Molecular logic of neocortical projection neuron specification, development and diversity. Nat. Rev. Neurosci. *14*, 755–769.
3. Lodato, S., and Arlotta, P. (2015). Generating neuronal diversity in the mammalian cerebral cortex. Annu. Rev. Cell Dev. Biol. *31*, 699–720.
4. Molyneaux, B.J., Arlotta, P., Menezes, J.R.L., and Macklis, J.D. (2007). Neuronal subtype specification in the cerebral cortex. Nat. Rev. Neurosci. *8*, 427–437.
5. Paolino, A., Fenlon, L.R., Suárez, R., and Richards, L.J. (2018). Transcriptional control of long-range cortical projections. Curr. Opin. Neurobiol. *53*, 57–65.
6. Srinivasan, K., Leone, D.P., Bateson, R.K., Dobreva, G., Kohwi, Y., Kohwi-Shigematsu, T., Grosschedl, R., and McConnell, S.K. (2012). A network of genetic repression and derepression specifies projection fates in the developing neocortex. Proc. Natl. Acad. Sci. USA *109*, 19071–19078.
7. Leone, D.P., Srinivasan, K., Chen, B., Alcamo, E., and McConnell, S.K. (2008). The determination of projection neuron identity in the developing cerebral cortex. Curr. Opin. Neurobiol. *18*, 28–35.
8. Rojo, C., Leguey, I., Kastanauskaite, A., Bielza, C., Larrañaga, P., DeFelipe, J., and Benavides-Piccione, R. (2016). Laminar Differences in Dendritic Structure of Pyramidal Neurons in the Juvenile Rat Somatosensory Cortex. Cereb. Cortex *26*, 2811–2822.
9. Oberlaender, M., de Kock, C.P.J., Bruno, R.M., Ramirez, A., Meyer, H.S., Dercksen, V.J., Helmstaedter, M., and Sakmann, B. (2012). Cell type-specific three-dimensional structure of thalamocortical circuits in a column of rat vibrissal cortex. Cereb. Cortex *22*, 2375–2391.
10. Ciganok-Hückels, N., Jehasse, K., Kricsfalussy-Hrabár, L., Ritter, M., Rüland, T., and Kampa, B.M. (2023). Postnatal development of electrophysiological and morphological properties in layer 2/3 and layer 5 pyramidal neurons in the mouse primary visual cortex. Cerebr. Cortex *33*, 5875–5884.
11. Larsen, D.D., and Callaway, E.M. (2006). Development of layer-specific axonal arborizations in mouse primary somatosensory cortex. J. Comp. Neurol. *494*, 398–414.
12. Kroon, T., van Hugte, E., van Linge, L., Mansvelder, H.D., and Meredith, R.M. (2019). Early postnatal development of pyramidal neurons across layers of the mouse medial prefrontal cortex. Sci. Rep. *9*, 5037.
13. Tjia, M., Yu, X., Jammu, L.S., Lu, J., and Zuo, Y. (2017). Pyramidal Neurons in Different Cortical Layers Exhibit Distinct Dynamics and Plasticity of Apical Dendritic Spines. Front. Neural Circ. *11*, 43.
14. Koester, S.E., and O'Leary, D. (1992). Functional classes of cortical projection neurons develop dendritic distinctions by class-specific sculpting of an early common pattern. J. Neurosci. *12*, 1382–1393.
15. Lodato, S., Molyneaux, B.J., Zuccaro, E., Goff, L.A., Chen, H.H., Yuan, W., Meleski, A., Takahashi, E., Mahony, S., Rinn, J.L., et al. (2014). Gene co-regulation by Fezf2 selects neurotransmitter identity and connectivity of corticospinal neurons. Nat. Neurosci. *17*, 1046–1054.
16. Molyneaux, B.J., Arlotta, P., Hirata, T., Hibi, M., and Macklis, J.D. (2005). Fezl is required for the birth and specification of corticospinal motor neurons. Neuron *47*, 817–831.
17. Chen, J.G., Rasin, M.R., Kwan, K.Y., and Sestan, N. (2005). Zfp312 is required for subcortical axonal projections and dendritic morphology of deep-layer pyramidal neurons of the cerebral cortex. Proc. Natl. Acad. Sci. USA *102*, 17792–17797.
18. Chen, B., Schaevitz, L.R., and McConnell, S.K. (2005). Fezl regulates the differentiation and axon targeting of layer 5 subcortical projection neurons in cerebral cortex. Proc. Natl. Acad. Sci. USA *102*, 17184–17189.
19. Guo, C., Eckler, M.J., McKenna, W.L., McKinsey, G.L., Rubenstein, J.L.R., and Chen, B. (2013). Fezf2 expression identifies a multipotent progenitor for neocortical projection neurons, astrocytes, and oligodendrocytes. Neuron *80*, 1167–1174.
20. Kmet, M., Guo, C., Edmondson, C., and Chen, B. (2013). Directed differentiation of human embryonic stem cells into corticofugal neurons uncovers heterogeneous Fezf2-expressing subpopulations. PLoS One *8*, e67292.
21. Tantirigama, M.L.S., Oswald, M.J., Duynstee, C., Hughes, S.M., and Empson, R.M. (2014). Expression of the developmental transcription factor Fezf2 identifies a distinct subpopulation of layer 5 intratelencephalic-projection neurons in mature mouse motor cortex. J. Neurosci. *34*, 4303–4308.
22. Bartel, D.P. (2004). MicroRNAs: genomics, biogenesis, mechanism, and function. Cell *116*, 281–297.
23. Tomasello, U., Klingler, E., Niquille, M., Mule, N., Santinha, A.J., de Vevey, L., Prados, J., Platt, R.J., Borrell, V., Jabaudon, D., and Dayer, A. (2022). miR-137 and miR-122, two outer subventricular zone non-coding RNAs, regulate basal progenitor expansion and neuronal differentiation. Cell Rep. *38*, 110381.

24. Wagner, N.R., Sinha, A., Siththanandan, V., Kowalchuk, A.M., MacDonald, J.L., and Tharin, S. (2022). miR-409-3p represses Cited2 to refine neocortical layer V projection neuron identity. Front. Neurosci. *16*, 931333.

25. Nowakowski, T.J., Rani, N., Golkaram, M., Zhou, H.R., Alvarado, B., Huch, K., West, J.A., Leyrat, A., Pollen, A.A., Kriegstein, A.R., et al. (2018). Regulation of cell-type-specific transcriptomes by microRNA networks during human brain development. Nat. Neurosci. *21*, 1784–1792.

26. Cho, K.H.T., Xu, B., Blenkiron, C., and Fraser, M. (2019). Emerging Roles of miRNAs in Brain Development and Perinatal Brain Injury. Front. Physiol. *10*, 227.

27. Shu, P., Wu, C., Ruan, X., Liu, W., Hou, L., Fu, H., Wang, M., Liu, C., Zeng, Y., Chen, P., et al. (2019). Opposing Gradients of MicroRNA Expression Temporally Pattern Layer Formation in the Developing Neocortex. Dev. Cell *49*, 764–785.e4.

28. Cremisi, F. (2013). MicroRNAs and cell fate in cortical and retinal development. Front. Cell. Neurosci. *7*, 141.

29. Diaz, J.L., Siththanandan, V.B., Lu, V., Gonzalez-Nava, N., Pasquina, L., MacDonald, J.L., Woodworth, M.B., Ozkan, A., Nair, R., He, Z., et al. (2020). An evolutionarily acquired microRNA shapes development of mammalian cortical projections. Proc. Natl. Acad. Sci. USA *117*, 29113–29122.

30. Enright, A.J., John, B., Gaul, U., Tuschl, T., Sander, C., and Marks, D.S. (2003). MicroRNA targets in Drosophila. Genome Biol. *5*, R1.

31. John, B., Enright, A.J., Aravin, A., Tuschl, T., Sander, C., and Marks, D.S. (2004). Human MicroRNA targets. PLoS Biol. *2*, e363.

32. Betel, D., Wilson, M., Gabow, A., Marks, D.S., and Sander, C. (2008). The microRNA.org resource: targets and expression. Nucleic Acids Res. *36*, D149–D153.

33. Betel, D., Koppal, A., Agius, P., Sander, C., and Leslie, C. (2010). Comprehensive modeling of microRNA targets predicts functional non-conserved and non-canonical sites. Genome Biol. *11*, R90.

34. Agarwal, V., Bell, G.W., Nam, J.W., and Bartel, D.P. (2015). Predicting effective microRNA target sites in mammalian mRNAs. Elife *4*, e05005.

35. Friedman, R.C., Farh, K.K.H., Burge, C.B., and Bartel, D.P. (2009). Most mammalian mRNAs are conserved targets of microRNAs. Genome Res. *19*, 92–105.

36. Garcia, D.M., Baek, D., Shin, C., Bell, G.W., Grimson, A., and Bartel, D.P. (2011). Weak seed-pairing stability and high target-site abundance decrease the proficiency of lsy-6 and other microRNAs. Nat. Struct. Mol. Biol. *18*, 1139–1146.

37. Grimson, A., Farh, K.K.H., Johnston, W.K., Garrett-Engele, P., Lim, L.P., and Bartel, D.P. (2007). MicroRNA targeting specificity in mammals: determinants beyond seed pairing. Mol. Cell *27*, 91–105.

38. Lewis, B.P., Burge, C.B., and Bartel, D.P. (2005). Conserved seed pairing, often flanked by adenosines, indicates that thousands of human genes are microRNA targets. Cell *120*, 15–20.

39. Maragkakis, M., Reczko, M., Simossis, V.A., Alexiou, P., Papadopoulos, G.L., Dalamagas, T., Giannopoulos, G., Goumas, G., Koukis, E., Kourtis, K., et al. (2009). DIANA-microT web server: elucidating microRNA functions through target prediction. Nucleic Acids Res. *37*, W273–W276.

40. Papadopoulos, G.L., Reczko, M., Simossis, V.A., Sethupathy, P., and Hatzigeorgiou, A.G. (2009). The database of experimentally supported targets: a functional update of TarBase. Nucleic Acids Res. *37*, D155–D158.

41. Reczko, M., Maragkakis, M., Alexiou, P., Papadopoulos, G.L., and Hatzigeorgiou, A.G. (2011). Accurate microRNA Target Prediction Using Detailed Binding Site Accessibility and Machine Learning on Proteomics Data. Front. Genet. *2*, 103.

42. Liu, W., and Wang, X. (2019). Prediction of functional microRNA targets by integrative modeling of microRNA binding and target expression data. Genome Biol. *20*, 18.

43. Wong, N., and Wang, X. (2015). miRDB: an online resource for microRNA target prediction and functional annotations. Nucleic Acids Res. *43*, D146–D152.

44. Olena, A.F., and Patton, J.G. (2010). Genomic organization of microRNAs. J. Cell. Physiol. *222*, 540–545.

45. Hollos, P., John, J.M., Lehtonen, J.V., and Coffey, E.T. (2020). Optogenetic Control of Spine-Head JNK Reveals a Role in Dendritic Spine Regression. eNeuro *7*, 1–16.

46. Coffey, E.T. (2014). Nuclear and cytosolic JNK signalling in neurons. Nat. Rev. Neurosci. *15*, 285–299.

47. Castro-Torres, R.D., Busquets, O., Parcerisas, A., Verdaguer, E., Olloquequi, J., Ettcheto, M., Beas-Zarate, C., Folch, J., Camins, A., and Auladell, C. (2020). Involvement of JNK1 in Neuronal Polarization During Brain Development. Cells *9*, 1897.

48. Molyneaux, B.J., Goff, L.A., Brettler, A.C., Chen, H.H., Hrvatin, S., Rinn, J.L., and Arlotta, P. (2015). DeCoN: genome-wide analysis of *in vivo* transcriptional dynamics during pyramidal neuron fate selection in neocortex. Neuron *85*, 275–288.

49. Galazo, M.J., Emsley, J.G., and Macklis, J.D. (2016). Corticothalamic Projection Neuron Development beyond Subtype Specification: Fog2 and Intersectional Controls Regulate Intraclass Neuronal Diversity. Neuron *91*, 90–106.

50. Beard, J.A., Tenga, A., Hills, J., Hoyer, J.D., Cherian, M.T., Wang, Y.D., and Chen, T. (2016). The orphan nuclear receptor NR4A2 is part of a p53-microRNA-34 network. Sci. Rep. *6*, 25108.

51. Jin, Y., Chen, Z., Liu, X., and Zhou, X. (2013). Evaluating the microRNA targeting sites by luciferase reporter gene assay. Methods Mol. Biol. *936*, 117–127.

52. Chai, F., Peng, H., Qin, L., Liu, C., Zeng, Y., Wang, R., Xu, G., Wang, R., Wei, G., Huang, H., et al. (2024). MicroRNA miR-181d-5p regulates the MAPK signaling pathway by targeting mitogen-activated protein kinase 8 (MAPK8) to improve lupus nephritis. Gene *893*, 147961.

53. Safa, A., Abak, A., Shoorei, H., Taheri, M., and Ghafouri-Fard, S. (2020). MicroRNAs as regulators of ERK/MAPK pathway: A comprehensive review. Biomed. Pharmacother. *132*, 110853.

54. Raffaele, I., Silvestro, S., and Mazzon, E. (2023). MicroRNAs and MAPKs: Evidence of These Molecular Interactions in Alzheimer's Disease. Int. J. Mol. Sci. *24*, 4736.

55. Jabaudon, D., Shnider, S.J., Macklis, J.D., Tischfield, D.J., and Galazo, M.J. (2012). RORβ Induces Barrel-like Neuronal Clusters in the Developing Neocortex. Cereb. Cortex *22*, 996–1006.

56. Björkblom, B., Östman, N., Hongisto, V., Komarovski, V., Filén, J.J., Nyman, T.A., Kallunki, T., Courtney, M.J., and Coffey, E.T. (2005). Constitutively active cytoplasmic c-Jun N-terminal kinase 1 is a dominant regulator of dendritic architecture: role of microtubule-associated protein 2 as an effector. J. Neurosci. *25*, 6350–6361.

57. Komulainen, E., Zdrojewska, J., Freemantle, E., Mohammad, H., Kulesskaya, N., Deshpande, P., Marchisella, F., Mysore, R., Hollos, P., Michelsen, K.A., et al. (2014). JNK1 controls dendritic field size in L2/3 and L5 of the motor cortex, constrains soma size, and influences fine motor coordination. Front. Cell. Neurosci. *8*, 272.

58. Komulainen, E., Varidaki, A., Kulesskaya, N., Mohammad, H., Sourander, C., Rauvala, H., and Coffey, E.T. (2020). Impact of JNK and Its Substrates on Dendritic Spine Morphology. Cells *9*, 440.

59. Runge, K., Cardoso, C., and de Chevigny, A. (2020). Dendritic Spine Plasticity: Function and Mechanisms. Front. Synaptic Neurosci. *12*, 36.

60. Hering, H., and Sheng, M. (2001). Dendritic spines: structure, dynamics and regulation. Nat. Rev. Neurosci. *2*, 880–888.

61. Holtmaat, A.J.G.D., Trachtenberg, J.T., Wilbrecht, L., Shepherd, G.M., Zhang, X., Knott, G.W., and Svoboda, K. (2005). Transient and Persistent Dendritic Spines in the Neocortex In Vivo. Neuron *45*, 279–291.

62. Hayashi, Y., and Majewska, A.K. (2005). Dendritic Spine Geometry: Functional Implication and Regulation. Neuron *46*, 529–532.

63. Grutzendler, J., Kasthuri, N., and Gan, W.-B. (2002). Long-term dendritic spine stability in the adult cortex. Nature *420*, 812–816.

64. Tsyporin, J., Tastad, D., Ma, X., Nehme, A., Finn, T., Huebner, L., Liu, G., Gallardo, D., Makhamreh, A., Roberts, J.M., et al. (2021). Transcriptional repression by FEZF2 restricts alternative identities of cortical projection neurons. Cell Rep. *35*, 109269.

65. Zuccotti, A., Le Magueresse, C., Chen, M., Neitz, A., and Monyer, H. (2014). The transcription factor *Fezf2* directs the differentiation of neural stem cells in the subventricular zone toward a cortical phenotype. Proc. Natl. Acad. Sci. USA *111*, 10726–10731.

66. Harris, K.D., and Shepherd, G.M.G. (2015). The neocortical circuit: themes and variations. Nat. Neurosci. *18*, 170–181.

67. Klein, A.M., Zaganjor, E., and Cobb, M.H. (2013). Chromatin-tethered MAPKs. Curr. Opin. Cell Biol. *25*, 272–277.

68. Tiwari, V.K., Stadler, M.B., Wirbelauer, C., Paro, R., Schübeler, D., and Beisel, C. (2011). A chromatin-modifying function of JNK during stem cell differentiation. Nat. Genet. *44*, 94–100.

69. Iyer, A.N., Bellon, A., and Baudet, M.L. (2014). microRNAs in axon guidance. Front. Cell. Neurosci. *8*, 78.

70. Leung, A.K.L. (2015). The Whereabouts of microRNA Actions: Cytoplasm and Beyond. Trends Cell Biol. *25*, 601–610.

71. Hu, Z., and Li, Z. (2017). miRNAs in synapse development and synaptic plasticity. Curr. Opin. Neurobiol. *45*, 24–31.

72. Barca-Mayo, O., and De Pietri Tonelli, D. (2014). Convergent microRNA actions coordinate neocortical development. Cell. Mol. Life Sci. *71*, 2975–2995.

73. Qu, C., Li, W., Shao, Q., Dwyer, T., Huang, H., Yang, T., and Liu, G. (2013). c-Jun N-terminal kinase 1 (JNK1) is required for coordination of netrin signaling in axon guidance. J. Biol. Chem. *288*, 1883–1895.

74. Fazeli, A., Dickinson, S.L., Hermiston, M.L., Tighe, R.V., Steen, R.G., Small, C.G., Stoeckli, E.T., Keino-Masu, K., Masu, M., Rayburn, H., et al. (1997). Phenotype of mice lacking functional Deleted in colorectal cancer (Dcc) gene. Nature *386*, 796–804.

75. Ha, H.-Y., Cho, I.H., Lee, K.W., Lee, K.W., Song, J.Y., Kim, K.S., Yu, Y.M., Lee, J.K., Song, J.S., Yang, S.D., et al. (2005). The axon guidance defect of the telencephalic commissures of the JSAP1-deficient brain was partially rescued by the transgenic expression of JIP1. Dev. Biol. *277*, 184–199.

76. Galazo, M.J., Sweetser, D.A., and Macklis, J.D. (2023). Tle4 controls both developmental acquisition and early post-natal maturation of corticothalamic projection neuron identity. Cell Rep. *42*, 112957.

77. Arlotta, P., Molyneaux, B.J., Chen, J., Inoue, J., Kominami, R., and Macklis, J.D. (2005). Neuronal subtype-specific genes that control corticospinal motor neuron development *in vivo*. Neuron *45*, 207–221.

78. Buenrostro, J.D., Wu, B., Chang, H.Y., and Greenleaf, W.J. (2015). ATAC-seq: A Method for Assaying Chromatin Accessibility Genome-Wide. Curr. Protoc. Mol. Biol. *109*, 21.29.1–21.29.9.

79. Li, Q., Brown, J.B., Huang, H., and Bickel, P.J. (2011). Measuring reproducibility of high-throughput experiments. Ann. Appl. Stat. *5*, 1752–1779.

80. Robinson, J.T., Thorvaldsdóttir, H., Winckler, W., Guttman, M., Lander, E.S., Getz, G., and Mesirov, J.P. (2011). Integrative genomics viewer. Nat. Biotechnol. *29*, 24–26.

81. Mi, H., Huang, X., Muruganujan, A., Tang, H., Mills, C., Kang, D., and Thomas, P.D. (2017). PANTHER version 11: expanded annotation data from Gene Ontology and Reactome pathways, and data analysis tool enhancements. Nucleic Acids Res. *45*, D183–D189.

82. Ventura, A., Meissner, A., Dillon, C.P., McManus, M., Sharp, P.A., Van Parijs, L., Jaenisch, R., and Jacks, T. (2004). Cre-lox-regulated conditional RNA interference from transgenes. Proc. Natl. Acad. Sci. USA *101*, 10380–10385.

83. Saito, T., and Nakatsuji, N. (2001). Efficient gene transfer into the embryonic mouse brain using *in vivo* electroporation. Dev. Biol. *240*, 237–246.

84. Vaasjo, L.O., Han, X., Thurmon, A.N., Tiemroth, A.S., Berndt, H., Korn, M., Figueroa, A., Reyes, R., Feliciano-Ramos, P.A., and Galazo, M.J. (2022). Characterization and manipulation of Corticothalamic neurons in associative cortices using Syt6-Cre transgenic mice. J. Comp. Neurol. *530*, 1020–1048.

STAR★METHODS

KEY RESOURCES TABLE

REAGENT or RESOURCE	SOURCE	IDENTIFIER
Antibodies		
chicken anti-GFP	Aves	Cat# 1020; RRID:AB_10000240
goat FITC conjugated anti-GFP	Abcam	Cat# ab6662; RRID:AB_305635
mouse anti-MAPK8	ProteinTech	Cat# 66210-1; RRID:AB_2881601
mouse anti-MAPK8	Abcam	Cat# ab129377; RRID:AB_11155905
Anti-mouse CY3	Thermo Fisher Scientific	Cat# A10521; RRID: AB_10373848
Goat anti-rabbit Alexa Fluor 488	Invitrogen	Cat#;A11008; RRID:AB_143165
Goat anti-rabbit Alexa Fluor 647	Invitrogen	Cat#A-21235; RRID:AB_2535804
Rabbit anti-HA	Covance	Cat# MMS-101R; RRID:AB_291262
Bacterial and virus strains		
Lenti-miR-193b; pSicoR backbone	Viral package by Systems Biosciences (Palo Alto, CA)	N/A
Lenti-miR-365; pSicoR backbone	Viral package by Systems Biosciences (Palo Alto, CA)	N/A
Lenti antisense miR-193b; pSicoR backbone	Viral package by Systems Biosciences (Palo Alto, CA)	N/A
Lenti antisense miR-365; pSicoR backbone	Viral package by Systems Biosciences (Palo Alto, CA)	N/A
Lenti scramble; pSicoR backbone	Viral package by Systems Biosciences (Palo Alto, CA)	N/A
Critical commercial assays		
TD Tagmented DNA buffer	Illumina	Cat # 15027866
TDE1 Tagment DNA enzyme	Illumina	Cat# 15027865
miRVana microRNA isolation kit	Ambion	Cat# AM1560
mRNA 1st-strand synthesis kit	Agilent	Cat# 600036
pmir-GLO reporter-miRNA oligo- DharmaFECT Duo	Dharmacon	Cat# T-2010
Anti Prominin 1+ MicroBeads	Miltenyi Biotec	Cat# 130-092-333
TD Tagmented DNA buffer	Illumina	Cat # 15027866
Deposited data		
ATAC-seq CSMN and CPN	This paper	GEO: GSE260574
Experimental models: Cell lines		
Neuro 2A cell line from mouse	Sigma Aldrich	Cat# 89121404; RRID:CVCL_0470
COS 7 cells	ATCC	Cat: CRL-1651; RRID:CVCL_0224
Experimental models: Organisms/strains		
CD-1 IGS wildtype	Charles River	Stock 022
Oligonucleotides		
primer- Fezf2 Forward- ACCCAGCTTCCTATCCCCAT	This paper	N/A
primer- Fezf2 Reverse GAGCATTGAACACCTTGCCG	This paper	N/A
primer- Mapk8 Forward CGCCTTATGTGGTGACTCGCTA	This paper	N/A
primer- Mapk8 Reverse TCCTGGAAAGAGGATTTTGTGGC	This paper	N/A
mmu-365a specific primer: CG-TAATGCCCCTAAAAATCCTT	This paper	N/A
mmu-miR-193b specific primer: CCCACAAAGTCCCGCTAAA	This paper	N/A

(*Continued on next page*)

Continued

REAGENT or RESOURCE	SOURCE	IDENTIFIER
Recombinant DNA		
pCAG-Fezf2	Molyneaux et al., 2005[16]	N/A
pCAG-miR-193b	This paper	N/A
pCAG-miR-365	This paper	N/A
pCAG-miR-scrambled	This paper	N/A
pCAG-HA-Fezf2-ires-GFP	Galazo et al., 2023[76]	N/A
Software and algorithms		
Prism	GraphPad	RRID:SCR_002798
Fiji ImageJ	Image J-NIH	RRID:SCR_002285
Neurolucida 360	MBF Bioscience	RRID:SCR_016788
Neurolucida Explorer	MBF Bioscience	RRID:SCR_017348
MATLAB 2001b	MathWorks	RRID:SCR_001622

EXPERIMENTAL MODEL AND STUDY PARTICIPANT DETAILS

All animal experiments were performed in accordance with Tulane University and Stanford University Institutional Animal Care and Use Committee's policies, and approved protocols, and following institutional and federal guidelines.

Cell lines

COS7 cells (ATCC, Cat: CRL-1651; RRID:CVCL_0224) and N2A (Neuro-2a) (ATCC, Cat #CCL-131; RRID:CVCL_0470) were cultured in DMEM-high glucose supplemented with 10 % FBS and 1% Penicillin-Streptomycin at 37°C and 5% CO_2.

Mouse lines

Time-pregnant wild-type female mice (CD-1 IGS; Stock 022) were purchased from Charles River Laboratories and used for in-utero electroporation experiments. Animals were maintained on a 12-hour light/dark cycle with free access to food and water.

METHOD DETAILS

Corticospinal projection neuron and callosal projection neuron FACS-purification

Corticospinal projection neurons and callosal projection neurons were purified from C57BL/6J mice as previously described.[49,77] Briefly, corticospinal projection neurons were retrogradely labeled at P1 from the cerebral peduncle by injection of cholera toxin B subunit (CTB) from *Vibrio cholerae* with FITC conjugate (List Biological Laboratories, Campbell, CA) under ultrasound microscopic guidance. At P2, neuron bodies in the motor cortex were isolated by microdissection of deep cortical layers, and dissociated to a single cell suspension by papain digestion and mechanical trituration. Callosal projection neurons were retrogradely labeled on P1 by injection of CTB into the contralateral hemisphere under ultrasound microscopic guidance. On P2, labeled cortices were microdissected and dissociated to a single cell suspension by papain digestion and mechanical trituration. FACS purifications were performed by the Stanford Shared FACS Facility. For differential miRNA expression analysis, neurons in suspension were FACS-purified into RNAlater (Life Technologies) using a FACS Vantage sorter (BD), and purified labeled neuron cell bodies were then frozen at -80°C until RNA purification. For ATAC-seq library preparation, the neuron suspensions were sorted into cold 50/50 media (50% DMEM, Life Tech 10569-010 and 50% Neural Basal Media, Life Tech 21103-049) for immediate processing.

RNA purification

microRNA was extracted from purified projection neuron cell bodies using the Ambion miRVana microRNA isolation kit (Ambion, Austin, TX) according to the manufacturer's instructions. RNA quality was analyzed on a BioAnalyzer 2100 (Agilent).

ATAC-seq library preparation and sequencing

Preparation of ATAC-seq libraries from viable cells has previously been described.[78] Briefly, viable FACS-sorted cells, 50,000 per biological replicate, were lysed in non-ionic detergent to isolate the nuclei. The nuclei were suspended in a transposition mix (TD Tagment DNA Buffer, Illumina Catalog No. 15027866, and TDE1 Tagment DNA Enzyme, Illumina Catalog No. 15027865), and incubated at 37°C to generate DNA fragments. After purification (Qiagen MinElute PCR purification Kit) the DNA fragments could be stored at -20°C. The DNA fragments were amplified using indexing primers, where the required number of PCR cycles is determined by qPCR (the required cycles were 25% of maximum fluorescent intensity). The product was purified once more to give the final library. Library concentrations were in the nano-molar range. The library quality was assessed using a BioAnalyzer (2100 Agilent, Stanford Functional Genomics Core). Samples with an RNA integrity number above 9 were used for ATAC-seq library sequencing. ATAC-seq

libraries were sequenced by the Stanford Functional Genomics Core on an Illumina MiSeq Sequencer. Each library produced approximately 200M, 150-bp paired-end reads. ATAC-seq data have been deposited in the Gene Expression Omnibus (GEO) database with accession no. GSE260574.

ATAC-seq analysis

The ENCODE ATAC-seq uniform processing pipeline v1.4.2 was used for replicated and unreplicated data (https://www.encodeproject.org/atac-seq/). The singularity-based pipeline for automated end-to-end quality control and processing of ATAC-seq data was installed from GitHub (https://github.com/ENCODE-DCC/atac-seq-pipeline). Alignments of paired-end fastq reads were performed against the mouse mm10 reference. A statistical procedure called the Irreproducible Discovery Rate (IDR), which operates on the replicated peak set and compares consistency of ranks of these peaks in individual replicate/pseudoreplicate peak sets, was used to generate a higher confidence, reproducible set of peaks with low false positive rates.[79] IDR can operate on peaks across a pair of true replicates resulting in a "conservative" output peak set, or across a pair of pseudoreplicates resulting in an "optimal" output peak set. These IDR conservative/optimal peaks for true/pseudo replicates respectively were then viewed on the Integrative Genomics Viewer (IGV).[80]

miRNA target prediction and Gene Ontology (GO) analysis

We used miRanda,[30–33] Targetscan,[34–38] DIANALAB,[39–41] and miRDB[42,43] to search for predicted miRNA targets. GO analysis was performed using the Panther GO tool.[81]

Quantitative PCR (qPCR)

Differential expression of miRNAs in corticospinal projection neurons and callosal projection neurons was analyzed via qPCR from purified P2 corticospinal projection neurons and callosal projection neurons using sno202 as a control. Relative Quantity (RQ) was calculated for each of the miRNAs, with $RQ = 2^{-\Delta\Delta Ct}$, providing a measure of the fold difference in miRNA expression by one cell type vs. the other.

For miRNA expression analysis after *Fezf2* and *Fezf2* shRNA expression in N2A cells and neurons, miRNAs were isolated using miRVana isolation kit (Ambion), cDNA was prepared using Agilent mRNA 1st-strand synthesis kit (Agilent, Cat. 600036) following manufacturer's instructions, followed by qPCR $2^{-\Delta\Delta Ct}$ method, using U6 as control and the following primers for miR-193b and miR-365:

mmu-365a specific primer: CG-TAATGCCCCTAAAAATCCTT

mmu-miR-193b specific primer: CCCACAAAGTCCCGCTAAA

Fezf2 shRNA sequence used: TTTAAATCCA-GTGCGCTGAAACATATTTAAT-TCCAGGCCTC Cloned into pAAV (Vector Builder).

For qPCR analysis of *Fezf2* and *MapK8* was performed using PerfeCTa SYBR Green SuperMix (Quantabio, 95071) on CFX96 system (Bio-Rad) was used with primers:

Fezf2 Forward ACCCAGCTTCCTATCCCCAT

Fezf2 Reverse GAGCATTGAACACCTTGCCG

Mapk8 Forward CGCCTTATGTGGTGACTCGCTA

Mapk8 Reverse TCCTGGAAAGAGGATTTTGTGGC

Experiments were performed in triplicates.

ChiP-qPCR

For ChIP-FEZF2 analysis *in utero* electroporation was performed at E13 with pCAG-HA-FEZF2-ires-GFP expression plasmid.[76] Corticospinal neurons or callosal projection neurons were retrogradely labeled from at P1 from the cerebral peduncle or the contralateral cortex with CTB-Alexa fluor 555. At P2, labeled cortices were dissected as described above to sort corticospinal and callosal projection neurons. ChIP using anti-HA antibody or non-specific IgG was performed in purified corticospinal and callosal neurons followed by qPCR as described in.[76] qPCR was performed using PerfeCTa SYBR Green SuperMix (Quantabio, 95071) on CFX96 system (Bio-Rad). Fold enrichment of anti-HA pull-down over IgG on each neuron population was analyzed in five different loci in the region upstream of the miR-193b-365 using the delta-Ct method. Primers used for amplicon detection:

ChiP-Fezf2 fw1 AGTCTAAATGGCAGAGCGGT; ChiP-Fezf2 rv1 AGCACATCCACCAATCCAGA

ChiP-Fezf2 fw2 AGCCCTATTTCCAGAGCCTG; ChiP-Fezf2 rv2 AGTTACTCCCAAACCCACCC

ChiP-Fezf2 fw3 GTGGCAGTTTCGTCTCTTGG; ChiP-Fezf2 rv3 CGGTCACTCGCATTCCTAGA

ChiP-Fezf2 fw4 CACAGTGGCAGTTTCGTCTC; ChiP-Fezf2 rv4 TCCAGATACAGTTGCGGTCA

ChiP-Fezf2 fw5 GCAGCTTACTACCTTCCCCT; ChiP-Fezf2 rv5 ACTTGGTGTCGTCTCAGTCC

Luciferase assays

Luciferase reporter assays were performed using the Dual-Glo Luciferase Assay System (Promega), pmir-GLO based reporter constructs, and microRNA oligonucleotides (Horizon Discovery) according to the manufacturer's instructions, as previously described.[29,50,51] Briefly, COS7 cells (10^4/well) were seeded in a white 96-well plate. The following day, pmir-GLO reporter-miRNA oligo- DharmaFECT Duo (Dharmacon) transfection mixtures were prepared. The media from the 96-well plate was replaced with the transfection mixture, and the plate was incubated overnight. Firefly and renilla luciferase reporter fluorescence was read using a

Tecan Infinite M1000 (Stanford High-Throughput Bioscience Center Core Facility). The ratio of firefly to renilla fluorescence was calculated for each well. Averages were compared for triplicates of each condition. Match reporter vectors contained the two wild-types predicted miR-193b (TACATTATTGGCCAGTTTCTGCCGCA) or miR-365 (ATAGGGCATTGAAGCAGAAA) seed regions with 30bp of flanking MapK8 3'UTR on either side of each. Mismatch reporter vectors were identical to match reporters except that the seed sequences were replaced by GGGGGGG. The experiments were replicated in n=5 independent cultures.

Lentivirus vectors

Lentivirus vectors were modified from the pSicoR backbone,[82] a gift from Tyler Jacks (Addgene plasmid # 11579). Expression of miRNA was under direction of the strong U6 promoter. miRNA inserts were: miR-193b (gain of function: AACTGGCCCTCAAA GTCCCGCTTTTTT), antisense miR-193b (loss of function: AGCGGGACTTTGTGGGCCAGTTTTTTT), miR-365 (gain of function: TAATGCCCCTAAAAATCCTTATTTTTT), antisense miR-365 (loss of function: ATAAGGATTTTTAGGGGCATTATTTTT), or scrambled (control, CCTAAGGTTAAGTCGCCCTCGCTCCGAGGGCGACTTAACCTTAGGTTTTT). All miRNA inserts were cloned between HpaI and XhoI sites. Expression of GFP was under direction of the CMV promoter. Lentivirus packaging was provided by System Biosciences (Palo Alto, CA). Titers of VSV-G pseudotyped viral particles were $\sim 10^7$ IFUS/mL.

Cell culture

Embryonic cortical cultures were prepared as previously described.[29] Briefly, E14 cortices were dissected and gently dissociated by papain digestion. A single cell suspension was prepared and plated onto poly-D-lysine (100μg/ml, Sigma) and laminin (20 μg/ml, Life Technologies) coated coverslips in cortical culture medium.

For progenitor selection, exclusion of Prominin 1+ cells was performed using Anti-Prominin1 MicroBeads (Miltenyi Biotec, 130-092-333). Cells were nucleofected (Amaxa, Lonza) with appropriate vector for each experiment and cultured on coverslips placed in 6-well plates for 5 days in growth media containing Neurobasal plus (Thermo Scientific, A3582901), supplemented with B-27, 1% Glutamax, 30% Glucose, and 1% penicillin-streptomycin at 37°C and 5% CO_2). Under these conditions, we observe >∼95% neurons and very few (<∼5%) astrocytes.

N2A (Neuro-2a) (ATCC, CCL-131) were cultured in DMEM-high glucose (Cytiva, SH30022) supplemented with 10 % FBS (Cytiva, SH3008803) and 1% Penicillin-Streptomycin (Thermo Fisher, 15070063) at 37°C and 5% CO2. Transfection of *Fezf2* expression plasmid[16] was performed using Lipofectamine 3000 following manufacturer's recommendations.

Immunocytochemistry of cultured cells

Cells were fixed with 4% paraformaldehyde (PFA) in PBS. Coverslips were blocked with PBS containing 0.1% Triton-X100, 2% sheep serum, and 1% BSA, and incubated with primary antibodies: mouse anti-MapK8 (Abcam, 1E5, dilution 1:200) and anti-GFP (Abcam, goat-FITC conjugated, dilution 1:250), and secondary antibodies conjugated with fluorophores: anti-mouse (Pierce, CY3-conjugate, dilution 1:1000). Cells were re-fixed in 4% PFA and washed thoroughly in ddH2O. The coverslips were then mounted using Fluoroshield with DAPI (Sigma) and imaged on a Zeiss AxioImager microscope.

Sholl analysis

Sholl analysis was performed to quantify neurite/dendritic complexity measuring the number of intersections of neurites with concentric circles surrounding the cell soma with radius increasing at 10 μm steps, for analysis of P14 neurons using Neurolucida software (MBF Bioscience), and 5 μm steps, for cultured neurons (using FIJI/IMAGEJ Sholl plugin). The number of intersections per radius increment was measured. ANOVA-Tukey was used to determine significant differences for Sholl analysis. Imaging acquisition and neuron reconstruction were performed blinded to the experimental conditions.

In utero electroporation

CD1 wild-type time pregnant females were obtained from Charles River. The day of vaginal plug detection was designated E0.5, and the day of birth as P0. For miR-365 and miR-193b gain-of-function experiments, a CAG/H1 promoter plasmid was used to drive expression of GFP and mature miRs. For control experiments, a similar plasmid was used to drive expression of GFP and a scrambled control microRNA (scrambled control). For expression of FEZF2-HA, we used previously plasmid.[76] *In utero* electroporation of embryonic mouse cortical neurons was carried out as previously described.[16] Briefly, 1μL of plasmid DNA at 1μg/μL mixed with 0.01% Fast Green was injected into the lateral ventricle of E13 (to target deep cortical layers) or E15 (to target superficial layers) CD1 mouse embryos *in utero*. Plasmids were electroporated into the neocortical ventricular zone using 5mm diameter platinum disk electrodes and a square-wave electroporator (BTX ECM 830) with five 30V pulses of 50 milliseconds duration at 950 millisecond intervals, as previously described.[83] Pups electroporated with FEZF2-HA were employed for ChIP-qPCR at P2, and pups electroporated with miR-365 and miR-193b constructs were collected for analysis at P14. Mice were processed for immunolabeling using standard intra-cardiac perfusion with 4% PFA.

Immunocytochemistry of brain sections

Pups were perfused at P14 with 4% PFA, and brains were post-fixed overnight in 4% PFA at 4°C. Brains for neuron reconstruction were vibratome sectioned coronally at 250 μm. Immunolabeling was performed to enhance GFP signal, incubated in primary

antibody for 48 hours (Rabbit anti-GFP 1:1000, Invitrogen) and in secondary antibody at 1:1000 for 5 hours at room temperature (Goat anti-rabbit Alexa Fluor 488, Invitrogen). Additional sections from the same brains containing electroporated somatosensory cortex were used for MAPK8 immunolabeling (mouse anti-MAPK8 1:200, Proteintech 66210-1; 48 hrs incubation) and in secondary antibody at 1:1000 for 5 hours at room temperature (Goat anti-rabbit Alexa Fluor 647, Invitrogen). Sections were mounted using Vectashield with DAPI. Additional electroporated brains were sectioned at 50 μm and processed for MAPK8 immunolabeling as described above.

Microscopy and image analysis

Images were acquired in a Nikon C2 confocal microscope at three magnifications. First, tile-scan epifluorescence images were acquired at 20x magnification to document the electroporated area. Then, z-stack tile-scan images containing multiple electroporated neurons in the somatosensory cortex were acquired with a 60x at 0.5 μm Z-resolution. Finally, z-stack images containing a single electroporated neuron with soma and basal dendrite in the somatosensory cortex were acquired with a 100x at 0.15 μm Z-resolution. All confocal images were Deconvolved using a Richardson-Lucy algorithm within 30 iterations using NIS Elements.

Neurons in the somatosensory cortex with strong GFP signal to detect third or higher order branching were selected for Sholl analysis. For dendritic spine analysis, 2nd order segments of apical dendrites and 3rd order segments of basal dendrites were selected for spine analysis. Spines were counted and classified semi-automatically, then manually curated by a trained investigator who was blinded to experimental conditions. Somas, dendrites, and dendritic spines were 3D-reconstructed using Neurolucida 360 (MBF Bioscience) and subjected to Sholl or Spine analysis using Neurolucida Explorer v.2021.1.1. (MBF Bioscience). ANOVA-Tukey was used to determine significant differences for Sholl analysis. ANOVA-Tukey was used to determine differences in spine density across groups, and one-tailed t-test to determine significant spine increase compared to control for single comparisons.

All imaging acquisition and neuron reconstructions were performed blinded to the experimental conditions.

For quantification of MAPK8 signal across layers, intensity profiles were performed as described in.[76] Briefly, 8-bit monochrome images corresponding to MAPK8 immunofluorescence signal were used. Intensity of MAPK8+ pixels was measured along the vertical lines spanning 450 μm from layer I into the cortical depth using the "Intensity Profile plot" function on ImageJ. Measurements from 10 vertical lines were averaged for each image. Images from at least three sections per brain were analyzed for each brain area. Fluorescence intensity in the white matter is constant across samples and was used for normalization.

For quantification of MAPK8 puncta in individual cells, Z-stack confocal images were acquired at 100x at 0.15 μm Z-resolution as in[84] and were analyzed with Neurolucida 360, Puncta analysis automated detection module (MBF Bioscience).

QUANTIFICATION AND STATISTICAL ANALYSIS

Details of imaging quantification methodologies are described in method details. All n values and p values obtained are listed in the figure legends. GraphPad Prism version 8 (GraphPad Software, Inc., San Diego, CA) or MATLAB R2021B (MathWorks, Inc) was used to perform statistical tests and graphs. Data distributions were assumed to be normal, but not formally tested. No statistical methods were used to pre-determine sample sizes.

We used unpaired Student's t-tests, Fisher's exact test, or ANOVA followed by Tukey post hoc test for statistical comparison. The specific test used for each analysis is indicated in the figure legends. Values are represented as means ± SEM. P-values are presented as follows; * $p<0.05$, ** $p<0.01$.